Variability of bottom carbonate chemistry over the deep coral reefs in the Florida Straits and the impacts of mesoscale processes

Mingshun Jiang[1*] Chudong Pan[1,#], Leticia Barbero[2], John Reed[1],
Joe Salisbury[3], James H. VanZwieten[4], and Rik Wanninkhof[2]

[1]Harbor Branch Oceanographic Institute, Florida Atlantic University

[2]Atlantic Oceanographic and Meteorological Laboratory, NOAA

[3]Ocean Process and Analysis Laboratory, University of New Hampshire

[4]Department of Civil, Environmental and Geomatics Engineering, Florida Atlantic University

for publication in

Ocean Modelling

*Corresponding author: jiangm@fau.edu, Telephone: 1-772-242-2254.
[#]Current address: NOAA, National Ocean Service, Silver Spring, MD 20910

Abstract

Abundant and diverse cold-water coral and fish communities can be found in the deep waters of the Florida Straits, which are believed to be living under suboptimal conditions impacted by increasing oceanic CO_2 levels. Yet, little is known regarding the spatial-temporal variability of bottom carbonate chemistry parameters and their dynamic drivers in this area. To address this issue, we present results from numerical simulations of a coupled physical-biogeochemical model for the south Florida shelf and Florida Straits. Our exploratory analysis focuses on two well-known deep-coral habitats: Pourtalès Terrace (200-450 m) and Miami Terrace (270-600 m). Results suggest that bottom waters along the northern/western slope of the Straits are comprised primarily of the North Atlantic Central Water (NWCW) and Antarctic Intermediate Water (AAIW), driven by upwelling associated with the bottom Ekman transport of the Florida Current. Over the Pourtalès Terrace, both the meandering of the Florida Current and mesoscale eddies modulate the upwelling (downwelling) of cold (warm) waters. In contrast, Florida Current makes a sharp turn at the southern end of the Miami Terrace leading to persistent island wakes, frequent occurrences of a transient eddy, and strong upwelling of deep waters toward the platform of the terrace. Passage of the transient eddy often accompanies strong downwelling of warm waters and a return (southward) flow on top of the platform. Overall, bottom water properties including temperature (T), dissolved inorganic carbon (DIC) and total alkalinity (TA) show strong variability on weekly to monthly time-scales over entire Pourtalès Terrace and on the platform of Miami Terrace mostly driven by physics. In deeper areas (>400 m), bottom water properties are fairly stable with both DIC and TA showing narrow ranges. Interestingly, waters over the southeastern portion of the Pourtalès Terrace show consistently warmer temperature, lower DIC, and higher TA than those on top of this terrace.

The aragonite saturation state (Ω) ranges 1.2-2 on top of the Pourtalès Terrace and 1.2-1.7 both on top of Miami Terrace and on the upper slope of Pourtalès Terrace. In the deeper slope areas (> 400 m), it is nearly constant at 1.2-1.3. This modeling effort suggests that remote forcing and biogeochemical processes along the transport paths, from the Gulf of Mexico to the Straits, are significant but second-order contributors to the variability of bottom carbonate chemistry. The impacts of benthic biogeochemical processes along the transit paths are not resolved.

Key words: coupled physical-biogeochemical model, mesoscale eddies, upwelling, aragonite saturation state, deep corals, Florida Straits

1. Introduction

In the North Atlantic Ocean, deep-sea coral ecosystems (DSCEs) are found most extensively off the coasts of Europe (Roberts, 2009 and reference therein) and the southeastern United States (SEUS), from North Carolina to Florida (Ross and Nizinski, 2007; Reed et al. 2005, 2006, 2013) (Figure 1). Off eastern Florida alone, it is estimated that deep-water coral habitats may extend over 13,440 km^2 (Reed et al. 2013). These DSCEs support diverse and abundant invertebrate and fish communities (Reed et al. 2005, 2006; Ross and Quattrini, 2007), and have been increasingly appreciated over the past decades as their extensive footprint is better understood. For example, the deep-water *Oculina* coral reefs off the east coast of Florida were the first deep-water Coral Habitat Areas of Particular Concern (CHAPC) in the world, designated by the National Oceanic Atmospheric Administration (NOAA) in 1984. Recently, NOAA designated five new deep-water CHAPCs in the SEUS, covering 62,714 km^2 (NOAA, 2010). The majority of these DSCEs occur within continental shelves and slopes, which are expected to experience the greatest changes in environmental stressors (e.g., temperature, pH) due to climate

change, ocean acidification, and deoxygenation on top of the large natural variability as compared to other portions of the deep-sea (e.g., Mora et al. 2013; Lunden et al. 2014; Perez et al. 2018).

It has been widely recognized that warming water temperatures and increasing CO_2 pose serious threats to the health of shallow coral reefs (e.g., Bellwood et al. 2004; Kleypas and Yates, 2009; Anthony et al. 2011). Less attention has been paid to deep-water reefs that are already living under high CO_2 conditions. The potential impacts of ocean acidification on deep corals and the deep coral ecosystems remains poorly understood (e.g., Hoegh-Guldberg et al. 2017). Limited experimental studies focused mainly on the growth and calcification rates of reef-building *Lophelia pertusa* and these results are mixed (e.g., Thresher et al. 2011; Maier et al. 2009, 2012; Lunden et al. 2014; Georgian et al. 2016a; Buscher et al. 2017; Gomez et al. 2018). The potential impacts may also include metabolism, reproduction capability, and the dissolution of coral reefs structures. Thus, it is important to better characterize the current mean state and variability of bottom carbonate chemistry over deep-water reefs. Significant progress has been made in observing environmental conditions of DSCEs including hydrodynamic and biogeochemical conditions (e.g., Mienis et al. 2012, 2014; Lunden et al. 2013; Ross et al. 2015; Georgian et al. 2016b). Yet information about carbonate chemistry conditions over the DSCEs remains scarce. This limits our capability to properly understand the potential threat of rising oceanic CO_2 to these communities. Limited studies suggest that the aragonite saturation state (Ω_{Ar}) is only marginally higher than 1.0 over the shelf slope in the Gulf of Mexico (GOM) and the Straits of Florida regions (Lunden et al. 2013; Wang et al. 2013; Wanninkhof et al. 2015). The three Gulf of Mexico and East Coast Carbon Cruises (GOMECC-1, 2 & 3) conducted in July 2007, 2012 and 2017, respectively, surveyed the same transect (27^oN) in the northern

Florida Straits yielding very similar Ω_{Ar} measurements, with values near the sea floor being only slightly higher than 1. For example, the minimum Ω_{Ar} was 1.19 and 1.36, respectively, for the west and east Florida slope during GOMECC2. Thus, progressive ocean acidification poses a significant threat to deep coral reefs by further lowering pH and reducing the availability of carbonate ions (CO_3^{2-}), particularly for aragonite, which is incorporated into scleractinian skeletons (Cohen and Holcomb, 2009; Perez et al. 2018).

Deep reef systems in this region are subjected to strong physical disturbances including upwelling, eddy entrainment and mixing, and the meandering of the Florida Current (FC). In the Straits of Florida the FC is the dominant current, with speeds that can exceed 2 m s^{-1}. This current originates from the Loop Current (LC) in the GOM and feeds into the Gulf Stream in the South Atlantic Bight. The FC impinges on the shelf of the Florida Keys and its core is mainly situated over the northwestern slope of the Straits, with persistent upwelling driven by the current-induced bottom Ekman transport (e.g., Pietrafesa, 1990; Garrett et al. 1993). The FC also exhibits mesoscale meanders with periods of 5 and 12 days and with wavelengths of, respectiveloy, 170 and 340 km (Johns and Schott, 1987), which can substantially vary the bottom temperature, salinity and velocities over these timescales. The FC also generates mesoscale (30-100 km) cyclonic eddies and sub-mesoscale (10-30 km) features along the shelf break (e.g., Lee, 1975; Lee and Mayer, 1977; Lee et al. 1995; Fratantoni et al. 1998). These dynamic features can further drive strong upwelling of CO_2-rich cold waters up the slope and onto the shelf (e.g., Smith, 1981; Pitts and Smith, 1997; Kourafalou and Kang, 2012; Xu et al. 2012), exposing the shelf fauna to cold, low pH, deep ocean waters.

In this manuscript we examine the temporal variability of key carbonate parameters including total dissolved inorganic carbon (DIC), total alkalinity (TA), pH, and Ω_{Ar}, in the deep

waters of the Florida Straits using a newly developed coupled physical-biogeochemical model and *in situ* measurements from shipboard surveys and bottom moorings. We focus on two key coral habitats, the Pourtalès Terrace and Miami Terrace (e.g., Reed et al. 2013, 2014). The Pourtalès Terrace lies in the southern slope of the Florida Keys, at depths between 200-450 m and a maximum width of 32 km. This 213 km long terrace consists of extensive, high relief, hard bottom, and essential fish habitats covering 3,429 km^2 (Figure 1). The southeastern flank of this terrace (between 81^{o}12´-80^{o}24´W) is located in the lee of Florida Current and is a CHAPC. Benthic communities on this terrace are dominated by stylasterid hydrocorals, gorgonian alcyonaceans, black corals, and sponges; the scleractinian corals include *Lophelia pertusa, Enallopsammia profunda, Madracis myriaster, Madrepora oculata, Solenosmilia variabilis,* and *Dendrophylliidae* and one *L. pertusa* mound was recently discovered on the Terrace slope (Reed et al. 2005, 2014). The fish communities consist of 62 species, including eleven commercially and recreationally important fish species (Reed et al. 2014). To the north of the Pourtalès Terrace is the Miami Terrace (25^{o}18'-26^{o}30'N), which extends 145 km long at depths from 275 to 600 m. The terrace covers 2,329 km^2 and has similar benthic biota as Pourtalès Terrace and *Lophelia/Enallopsammia* coral mounds and coral rubble are common at the foot of the escarpment (Reed et al. 2006; Vinick et al. 2012).

The objectives of this manuscript are two-fold: 1) further assessment of model skills in simulating the deep water upwelling, mesoscale eddies, and near bottom water properties in the Florida Straits, and 2) characterization of spatial-temporal variability of bottom water properties especially carbonate chemistry and controlling processes including mesoscale eddies and current meandering. The numerical model and *in situ* data used for assessing model skills are described in Section 2. Model results including a comparison with *in situ* data, key physical and carbonate

chemistry features, and the variability of near bottom water properties are presented in Section 3. In Section 4, key controlling processes for this variability are discussed, including meso- and submesoscale eddies and associated upwelling, large-scale transport and mixing, and biogeochemical processes such as local export and remineralization of organic carbon. Finally, some concluding remarks are made in Section 5.

2. Methods

2.1. Model

The numerical model is based on the Regional Ocean Modeling System (ROMS), a three-dimensional primitive equation ocean model system (e.g., Shchepetkin and McWilliams, 2005). The model domain covers the south Florida shelf, Florida Straits, northern Cuban coastal region and western Great Bahamas Bank, with a horizontal resolution ~ 1.5 km and 35 sigma layers vertically concentrating near the surface (Figure 1). The numerical schemes for momentum equations and tracers are third-order upstream for horizontal advection, and fourth-order centered difference for vertical advection. Vertical turbulent mixing is computed with the generic length scale (GLS) turbulent closure (Umlauf and Burchard, 2003). A uniform horizontal and viscosity and mixing coefficient of 10 m^2/sec were applied on the geopotential surfaces (Haidvogel and Beckmann, 1999). The model is driven by surface meteorological forcing derived from the 3-hourly North American Regional Reanalysis (NARR, Mesinger et al. 2006), open boundary forcing derived from the 1/25^o Gulf of Mexico Hybrid Coordinate Ocean Model (HYCOM, Chassignet et al. 2009) output, and the local run-off collected at the USGS gauges (http://waterdata.usgs.gov/nwis). Results presented in this manuscript are from a run without tidal forcing. Tides are important over the south Florida shelf and shelfbreak (e.g., Leichter et al. 2007) but tidal currents are moderate, ~20 cm/sec, over the mid to lower slope. Temperature

anomalies at tidal frequencies are small with the standard deviations at 0.16°C and 0.09°C, respectively, as observed at the T2 and T3 stations. In order to avoid drift of sea surface temperature (SST) on the continental shelf, particularly shallow areas, model SST is relaxed to observed daily SST from satellite observed SST (http://podaac.jpl.nasa.gov/). The modeled period was chosen as 2011-2012. More details for the physical model can be found in Pan et al. (2017). Unlike the previous simulations reported in Pan et al. (2017), the model bathymetry cut-off is now 2000 m instead of 1500 m.

The physical model is coupled with a biogeochemical model developed by Fennel et al. (2006, 2008), with some modifications made to parameter values (see Table 1). This model has six functional groups that describe the nitrogen cycle through the lower food web, nitrate (NO_3) and ammonia (NH_4), phytoplankton, zooplankton, small detritus and large detritus. Chlorophyll is a diagnostic variable based on the phytoplankton chlorophyll to carbon ratio, which is computed following the light acclimation model by Geider et al. (1998). It also includes DIC, dissolved oxygen (DO), and TA. In our implementation, we adjusted some key parameters such as light attenuation and half saturation constants (Table 1) in order to better simulate deep ocean phytoplankton dynamics, including the reproduction of the deep chlorophyll maximum. The simulation of the carbon cycle largely follows the nitrogen cycle, with a fixed Redfield carbon to nitrogen ratio of 6.625. The air-sea CO_2 flux is determined by the air-sea partial pressure of CO_2 (pCO_2) multiplied by the gas-transfer (or piston) velocity, which is computed following the formulation of Wanninkhof (1992). Alkalinity is assumed to be unaffected by air-sea gas exchange of CO_2, but instead altered by a number of biogeochemical processes, including calcite formation and dissolution, nitrate uptake and regeneration, and sulfate reduction. In this model, only the nitrate uptake and remineralization of organic nitrogen are included. Based on the model

output, pH and Ω_{Ar} were computed from DIC and TA using a Matlab co2sys package with K1 and K2 constants from Mehrback et al. (1973) and K_{SO4} from Dickson (1990) (see Lewis and Wallace, 1998; Van Heuven et al. 2011).

The biogeochemical parameters in the river inputs to the model include nutrients (NO_3, NH_4), dissolved organic matter, DIC and TA. There are only very limited measurements for biogeochemical parameters in the rivers. For simplicity, in this simulation we used constant values (5 μmol/l for NO_3, 4 μmol/l for NH_4, 120 μmol/kg for DOC, 2100 μmol/kg for DIC and 2300 μmol/kg for TA) based on the available data compiled by the South Florida Water Management District (http://my.sfwmd.gov/dbhydroplsql/show_dbkey_info.main_menu). This choice will affect the biogeochemical results including nutrients, phytoplankton biomass, DIC and TA in nearshore and coastal areas, but we do not expect it to significantly affect water properties in the offshore areas particularly bottom waters in the Florida Straits, where river influences are minimal. Construction of more detailed river inputs is currently underway.

The boundary conditions for nitrate, DIC and TA were prescribed based on their respective nonlinear regressions with temperature derived from observed concentrations along the west Florida Slope transect during GOMECC2 cruise (Figure 2). The boundary temperature field was derived from GOMex model output as described above. The assumption is that these water properties along the western boundary are generally similar because all waters in the GOM come from the subtropical North Atlantic through the Caribbean Sea (Rivas et al. 2005). Local physical-biogeochemical processes will undoubtedly modify the water properties. There is insufficient information to specify more detail (e.g., spatial gradients) along the boundary. The NO_3, DIC and TA concentrations are all strong correlated with both the temperature and salinity as observed along the western Florida shelf slope during GOMECC2 cruise (Figure S1). Yet,

both the NO_3 and DIC correlations with temperature (r=0.99 NO_3 and r=0.98 for DIC) for were much stronger than those with salinity (r=0.93 for NO_3 and r=0.9 for DIC), while the TA correlation with temperature was similar with that with salinity. Therefore, temperature was used to construct the model boundary conditions for the NO_3, DIC, and TA.

The boundary conditions for other biogeochemical variables are derived from the output of the coupled ROMS-CoSINE (Carbon, Silicon, Nitrogen Ecosystem) model developed by Dr. Chai at the University of Maine (Chai, *pers. comm.*). The CoSINE model was originally developed for the Pacific Ocean, but was adapted for the northwest Atlantic Ocean (Xiu and Chai, 2014). The model consists of 31 state variables describing 3 types of nutrients (N, P, Si), three phytoplankton functional groups (picoplankton, diatoms, and coccolithophorids), two size classes of zooplankton (microzooplankton, mesozooplankton), bacteria, several groups of organic matter, dissolved oxygen (DO), total alkalinity, and TCO_2. The model was coupled with a 7-km ROMS model with a domain covering the Northwest Atlantic region including the Gulf of Mexico. A 50-yr (1957-2007) simulation of the coupled model has been performed, and the physical model has been calibrated, indicating satisfactory model skills including capturing the Gulf Stream dynamics (Kang and Curchitser, 2013). No systematic calibration or validation, however, has yet been made for the biogeochemical simulation. We used the biogeochemical results from the last two years (2006-2007), an arbitrary choice, to derive biogeochemical boundary conditions for our modeling period (2011-2012) because the ROMS-CoSINE simulation for this period is not available. We do not, however, expect this temporal miss-match to significantly impact model calculations as the three key parameters (nitrate, DIC and TA) were specified separately from the CoSINE results. At present, we have no sufficient observed data for specifying other biological variables (PON/POC, DON/DOC, plankton biomass) in the

Gulf of Mexico. The justification of our choices for these boundary parameters is provided in the Supplement Materials, which include a figure showing the temporal variability of key biogeochemical variables along the western boundary on the west Florida Slope (Figure S3). The time mismatch in boundary conditions and lack of validation of the biological parameters means that the results should be viewed with a degree of uncertainty, due to the previously mentioned factors. As much of the carbon dynamics are driven by well-constrained physical variability in the domain the processes and patterns are representative of actual conditions.

2.2. Data

Extensive model calibration has been performed for the physical model using available data from various sources (Pan et al. 2017). In this manuscript we compare model results with data collected in the Florida Straits from four sources, which have not been used in the calibration by Pan et al. (2017): 1) integrated transport between west Palm Beach and Grand Bahamas Island (between 26-27^{o}N) through the northern Florida Straits (Meinen et al. 2010); 2) the second Florida Shelf-Edge Experiment (FloSEE) cruise, which took place in September 11-November 10, 2011; 3) the GOMECC2 cruise, which took place in July-August, 2012; and 4) near bottom temperature and current profiles measured by Acoustic Doppler Current Profilers (ADCPs) at two mooring stations on the Miami Terrace (Figure 1). We also compare the model output of biogeochemical variables with limited data collected during the FloSEE and GOMECC2 cruises.

The transport by Florida Current through the northern Florida Straits has been measured using various methods at around 27°N. Here, we use the estimates based on the voltage change to a submarine telephone cable due to the current-induced changes in magnetic field, which covered various periods from1970 to present (Meinen et al. 2010). The transport was calibrated

with the more accurate estimates based on the time lapse of a free falling dropsonde at a series of stations across the Straits that took place about once per month (Niiler and Richardson, 1973; Garcia et al. 2014). Tidal signals were removed from the final transport estimate.

The FloSEE cruise, onboard the NOAA ship *Nancy Foster*, focused on the Pulley Ridge mesophotic coral reef ecosystem on the southwest Florida shelf, with the objective of studying the potential impacts of the Deepwater Horizon oil spill event on south Florida coral reefs (Reed et al. 2012). In addition to benthic surveys (e.g., coral species, video of benthic habitats, images from side-scan sonars) with a Remotely Operated Vehicle (ROV), a Bluefin spray glider was deployed for measuring water properties (T, S) over the outer shelf of the southwest Florida shelf (see Pan et al. 2017). Traditional CTD casts were also made over Pulley Ridge, the Pourtalès Terrace (4 stations) and southern slope off Key West (1 station) (Figure 1). Water properties measured using a Sea-Bird 911plus CTD rosette system included temperature, salinity, turbidity, fluorescence, pH, and dissolve oxygen (DO). Collected data were binned into 1 m depth intervals. For this manuscript, we only used the data from the CTD stations over the Pourtalès Terrace.

The GOMECC cruises were funded by NOAA's Ocean Acidification Program (OAP), with cruises conducted in summers of 2007, 2012, and 2017 to measure hydrological and carbonate chemistry parameters in the Gulf of Mexico and U.S. East Coast (only first two cruises) (Wang et al. 2013; Wanninkhof et al. 2015). These cruises covered the GOM and US East Coast, with 18 transects that ran from the coast to deep oceans. Two other NOAA-sponsored cruises, East Coast Ocean Acidification (ECOA) I and II were conducted in 2015 and 2018, respectively, which occupied most of the GOMECC stations on the east coast, but with more detailed surveys in some selected coastal areas. During all of these cruises, a number of

physical-biogeochemical parameters were measured with bottled samples including temperature (T), salinity (S), chlorophyll (Chl), macro-nutrients, DIC, TA, and DO, among others. The analysis for chlorophyll samples was limited to the upper 250 m. Results from the first and second GOMECC cruises can be found in Wang et al. (2013) and Wanninkhof et al. (2015), respectively. Yang et al. (2015) examined the variability of total alkalinity in the northeastern Gulf of Mexico using the GOMECC2 data and other historical measurements. Here we will use the data from the bottle samples collected between July 22 – August 13, 2012 during GOMECC2 along two transects that are located inside our model domain: transect 1 extending from Tampa Bay to the shelf break (hereafter referred to as WFL), and transect 2 across the northern Florida Straits (hereafter referred to as EFL) along the Ft. Pierce, FL segment at 27°N (Figure 1). These data indicate strong nonlinear correlations between temperature, DIC, TA and NO_3 especially below the thermocline (Figure 2). In order to corroborate bottom water masses, we also use a portion of the data along A22 transect (~70^o-65^{o}W) of the WOCE survey, which took place in March 24-April 17, 2012 (http://whp-atlas.ucsd.edu/atlantic_index.htm). Data used below were from stations 66-81 between 12^{o}36-16^{o}19.7'N, which were within the Caribbean Current that feeds into the Gulf of Mexico.

To further evaluate the model predictions, particularly on the temporal dimension, we compare model output with observed time series of near-bottom (~12 meters above the sea floor) temperatures and current profiles. Between 2009 and 2015, ADCP moorings have been periodically deployed on the northern Miami Terrace (latitude ~ 26^{o}4′ N) at 4 locations from 260 m to 640 m (Figure 1). Two temperature time-series collected from moorings T2/B2 (320 m total water depth) and T3/B3 (290 m total water depth), and one water velocity time-series measured from mooring T2/B2 (measurement depth of 156 m) are utilized in this study. It is noted that the

temperature sensor elevation above the sea floor (~ 12 m) is similar to the water depth of the first model layer from the bottom. For more details about these instruments and measurements please see Machado et al. (2016).

3. Results

3.1. Model skills

Extensive calibration of the physical model has been conducted using the following four data sets (Pan et al. 2017): 1) FloSEE ship deployed CTD data, 2) CTD measurements onboard a Spray glider during two month-long surveys over western Florida Shelf, 3) satellite altimetry measured sea surface height (SSH), and 4) satellite infrared imaged sea surface temperature (SST). Results indicate that the model is able to reproduce the spatial-temporal variability of water properties, as well as key dynamic processes including LC/FC dynamics, formation and propagation of mesoscale eddies associate with the current instability, interactions between eddies and the shelf/slope, and upwelling associated with the eddies and LC/FC meandering (e.g., Johns and Schott, 1987; Kourafaou and Kang, 2012). This previous comparison, however, focuses on the west Florida shelf, particularly in the Pulley Ridge area. Here we provide an additional assessment on the model skills, with a focus on the Florida Straits (Figures 2-6). The relevant statistics of these model-data comparisons are shown in Table 2, where the last column shows the mean model-data differences along with the confidence interval based on the paired student-*t* test.

We first present the comparison between model and observed transport at 27^{o}N (Figure 3). The result indicates that the model captures the magnitude of volume transport along this section with mean transport at 30.3 vs 31.2 m^3/sec, both are close to recent estimates of the mean transport. However, for unclear reasons, the model under-estimates the variability of volume

transport on a monthly timescale (Figure 3a). Modeled variability of volume transport on shorter timescales (<11 day) due to meso- and submesoscale activities is similar to measured data, with standard deviation (std) at 0.8 m^3/sec for model vs 1.1 m^3/sec for data (Figure 3b). Model volume transport also has a weak correlation with measured data, with the correlation coefficient r=0.19 (p<0.05) and r=0.27 (p<0.01), respectively, for the low frequency (>11 day) and high frequency (<11 day) components.

A comparison of model and observed key parameters from July 30-31, 2012 along the GOMECC-2 EFL transect is shown in Figure 4. Both modeled results and observations indicate strong bottom upwelling of cold and relatively low salinity waters along the western slope (left side of the current looking downstream) of the transect, as shown in the upward tilting of the isotherms and isopleths of other water properties. This is consistent with the well-known feature of the Florida Current that its main axis is located mid-slope on the west side of the Straits (e.g., Seim et al. 1999). The modeled upwelling in this instance, however, is weaker than the observations, with the modeled temperature of the upper slope water about ~3^{o}C warmer than the measurements (Figure 4a and b). Upwelling was unusually strong during the GOMECC-2 cruise (Zhang et al. 2017). On average, however, model temperature along this transect is only about 0.3^{o}C lower than the observed, which is not statistically significant (Table 2). The model is also able to reproduce the general pattern of salinity including the high salinity subsurface layer between 50 – 300 m along the central-right flank of the Florida Current, which represents the North Atlantic salinity maximum waters (SMW) from the subtropical North Atlantic Ocean (see. e.g., Roson et al. 2003). Modeled salinity over the upper western slope is higher than the observed salinity by about 0.25 psu, but the average modeled salinity along this transect agrees

well with observations. Both model temperature and salinity show a strong point-to-point correlation with data (r=0.93 and 0.65, respectively) (Table 2).

A comparison between model and observed key biogeochemical parameters (DIC, nitrate and TA) along the same transect tells a similar story (Figure 4e-j). The model reproduces the general patterns and ranges of these parameters. However, over the upper slope modeled NO_3 and DIC concentrations are lower than the observed (Zhang et al. 2017), whereas modeled alkalinity is about 10-20 μmol/kg higher than the observed (Figure 4i-j) in accord with higher observed upwelling. The point-to-point correlation coefficients and root-mean-square error (RMSE) between the model and observed values are, respectively, 0.9 and 4.5 μmol/kg for nitrate, 0.96 and 20.4 μmol/kg for DIC, and 0.69 and 18.4 μmol/kg for TA (Table 2). On average, modeled DIC is 8 μmol/kg higher than the observed and modeled TA is 10 μmol/kg higher than the observed. The GOMECC measurement errors for DIC and TA are, respectively, 2 μmol/kg and 4 μmol/kg. Therefore we believe these mismatches are mostly due to model biases. Only a subset of water samples was analyzed for chlorophyll concentration. Along this transect, the data also clearly shows a subsurface maximum with increasing depth at around 30 m at the shelf edge to 100 m offshore, generally in agreement with the model vertical distribution. The overall a point-to-point correlation between model and data is r=0.37 (p<0.01) and r=0.74 after excluding a few outlier (see Figure S2).

The temporal variability of model temperature and current fields are compared with data collected from two ADCP moorings, T2 and T3 (Figure 5). Overall, the model reproduces near-bottom temporal patterns (e.g., dominant periods) reasonably well over weekly-to-monthly timescales. A simple spectral analysis indicates that the model and observed bottom temperatures at T2 and T3 have very similar power spectra with no obvious peak at low frequency (>11 day)

but prominent peaks at the 7-day period for high frequency variability (<11 days) (not shown). Modeled and observed temperatures at both locations have similar magnitudes in high frequency variability (Figure 5a, b). The model and observed stds are 0.52 and 0.67 ^{o}C, respectively, at T2, and 0.66 vs 0.68 ^{o}C, respectively, at T3. The model, however, over-estimates the magnitudes of low frequency variability at both locations, as reflected in the differences between modeled and observed standard deviations (Table 2).

The model and observed N-S velocities at T2 agree on the short-term variability in terms of both mean values and the amplitude of variability (Figure 5c, e; Table 2). Moreover, in the upper layer modeled N-S velocity strongly correlates with observed values (e.g., r=0.66 at 68 m). However, the model-data correlation decreases with depth. Both model and observed E-W velocities show a persistent eastward component, but the model average is only about 50-60% of the observed (Figure 5 d, f; Table 2). Also, the observed E-W velocity shows much stronger variability than the modeled. Comparisons of modeled and observed currents at other depths above this same location, and at two other mooring sites, yield similar conclusions (not shown).

As another check on modeled vertical structures of water properties, we compared model and observed temperature and salinity profiles at several stations over the Pourtalès Terrace during the FloSEE survey (Table 2). Modeled temperature agrees well with these measured data, with a correlation coefficient r=0.97. However, the model-data agreement for salinity is less strong (r=0.75). In particular, the model under-estimates salinity by 0.3-0.6 psu in the upper 150 m. Modeled chlorophyll profiles show a prominent subsurface chlorophyll maximum (SCM) at all of the FloSEE stations, which depth is quite variable between stations. No direct comparison, however, was made for the modeled chlorophyll with FLOSEE data, which only

reported fluorescence. The observed fluorescence, however, shows a consistent depth of maximum at ~65 m.

For all of these comparisons, model skills are quantitatively evaluated with three metrics: correlation coefficient (*r*), standard deviation (std), and normalized root mean squared error (RMSE). These can be summarized with the Taylor diagram as shown in Figure 6 (Taylor, 2001). Here "A" is the reference point representing the perfect match between model and data, and other letters represent the cases evaluated (Table 2). The closer the triad is to "A" the better model skill. It is clear that the poorest agreement is from the comparison with mooring data (cases K-P), indicating the challenge of the model in reproducing both the phase and magnitude of the temporal variability on small scales. Overall, this diagram indicates a reasonable performance of the model.

3.2. Upwelling driven by Florida Current and mesoscale eddies

Florida Current typically tilts up to the left flank due to the bottom Ekman transport and associated geostrophic adjustment (Figure 4). In a steady state, bottom friction acting on the current would lead to bottom Ekman transport, which moves to the left of the current and drives near bottom upwelling of nutrient-rich cold waters up the slope (Hsueh and O'Brien, 1976; Garrett et al. 1993; Seim et al. 1999: Zhang et al. 2017). Thus upwelling or downwelling due to current meandering and eddies will be superimposed on this background because variability in the Florida Current or the presences of eddies will change bottom Ekman transport, leading to enhanced upwelling or reduced upwelling, i.e. downwelling. Moreover, upwelling generally accompanies strong and persistent phytoplankton blooms near the slope area (e.g., Llopiz, 2008), which is also seen from our model results (not shown). The export of the organic matter

produced in these blooms can be critical food sources for the abundant deep corals found in the Straits.

The formation and evolution of mesoscale and sub-mesoscale eddies associated with the FC have been well documented (e.g., Lee, 1975; Lee and Mayer, 1977; Lee et al. 1995; Fratantoni et al. 1998; Kourafalou and Kang, 2012; Richardson et al. 2015). Elongated mesoscale and sub-mesoscale eddies with low temperatures near their cores are frequently produced locally or pass through this area. Elevated chlorophyll concentrations are frequently observed along the edge and near the center of these eddies using satellite images (e.g., Kourafalou and Kang, 2012). This model is able to produce similar mesoscale and sub-mesoscale eddies in the Straits, although sub-mesoscale activities might be under-represented in the model because of its relatively coarse model resolution (1.5 km). We will focus on mesoscale eddies in the following sections.

Modeled results suggest mesoscale eddies could have significant impacts on bottom water properties over the Pourtalès Terrace. As an example, we present a series of currents maps at 150 m and bottom temperature over the Pourtalès Terrace (Figure 7, left), as well as the companion vertical distributions of temperature and along-channel (W-E) velocity along the ~81°W transect across the shelf slope of Pourtalès Terrace (Figure 7, right). Between February 16-25, 2012, a mesoscale eddy passes through the area (Figure 7c, e, g). On Feb. 4, 2012, before the eddy, bottom temperature and 150 m currents indicate persistent cross-slope transport at the western end of the Pourtalès Terrace, leading to cold waters (~10^{o}C) residing over the inner side of the platform (Figure 7a, b). This is in addition to the upwelling driven by the bottom Ekman transport induced by the Florida Current, as noted above. As a result, bottom temperature over the outer slope of the terrace is typically warmer than on the platform. On Feb. 16, 2012, an eddy

is seen encountering the western edge of the terrace, which appears to have blocked cold-water intrusion onto the inner platform, but instead brings deep water directly through the outer slope (Figure 7c, d). The eddy takes about one week to propagate through the terrace. Both the leading front and eddy center drive strong upwelling, uplifting the isopycnals and flushing the terrace with deep cold waters (Figure 7e, f). After the eddy passes through the area, significant downwelling takes place along the trailing edge of the eddy, which flattens the thermocline and the western part of the terrace is covered with warmer waters (~16^{o}C) (Figure 7g, h). Thus, the temperature change over the terrace before and after the passage of the eddy is 3-7°C. A examination of model results over the two-year period suggest that similar events have happened 3 times in 2011 and 4 times in 2012, all occurring during spring and fall seasons.

3.3. Island wakes around the Miami Terrace

The dynamics of currents-bathymetry interactions over the Miami Terrace is different from those over the Pourtalès Terrace. This can be illustrated with a series of temperature and currents maps at 300 m (Figure 8, left panels) and temperature and N-S water velocity maps along a cross-slope transect at 25°25´N (Figure 8, right panel) for February 14-24, 2012. In this area, the Florida Current changes its direction from northeastward to northward, and therefore the current axis often meanders significantly. In the upper layer, however, the Florida Current typically follows the nearly straight N-S shelf slope. Thus, strong upwelling is primarily due to the bottom Ekman transport. In deeper areas, the bathymetry contour takes a sharp turn from northeast to north at around 25°12´N, and then another turn to the east at around 25°45´N. As a result, the left flank of the Florida Current frequently overshoots, creating island wakes with an area of low flow and significant upwelling over the Pourtalès Drift, an area between 25°N and the Miami Terrace (Figure 8 c-f). Consistent with our results, Kourafalou and Kang (2012) also

found that stronger upwelling takes place in this area as the core of the current shifts eastward away from the western slope. Unlike their analysis, which focused on the top 200 m, our focus here is deeper areas.

Clearly, the upwelled cold deep waters will be transported downstream toward the terrace. This effect can be illustrated in Figure 9, which shows the maps of bottom temperature and currents (Figure 9, left panels) and temperature and N-S velocity along a cross-slope transect at the south end of the Miami Terrace (25°40´N) (Figure 9, right panel) during the same period as in Figure 8. It is notable that the overshoot of Florida Current on February 18, 2012 leads to a cyclonic eddy of approximately 20 km wide and 50 km long in the wakes along with strong upwelling that further uplifts the thermocline (Figure 9c, d). The eddy propagates slowly downstream but only lasts a few days, disappearing within a 30-40 km distance of the spawning area (Figure 9e, f). An examination of modeled results over the 2-year period indicates frequent occurrences of this eddy, approximately once per week each lasting about 2-5 days.

The occurrence of this eddy significantly affects the bottom water properties over the Miami Terrace. Without an eddy, bottom water temperature on the platform is typically 2-4ºC warmer than over the slope (Figure 9a, b). When an eddy is present, both the isothermals over the center and along the leading edge of the eddy are further uplifted (Figure 8d, f and 9d, f), allowing more upwelling of cold waters over the platform and reducing the bottom temperature (Figure 9c, f). As the eddy propagates downstream, it induces significant downwelling of warmer upper layer waters in its wake (Figure 9g, h). Sometimes, a return flow at between 200-300 m water depth is present, likely due to the geostrophic adjustment. Soloviev et al. (2017) also noted the presences of an intermittent countercurrent down to 244 m over the Miami Terrace.

Island wakes and associated upwelling of deep cold waters are ubiquitous phenomena when oceanic currents encounter topographic obstacles in the deep oceans (e.g., Dong et al. 2007). In our case, this is largely a subsurface phenomenon because the wakes and eddy are mostly below the thermocline. Several previous studies have reported that a countercurrent (southward) existed between 400-700 m and 25°40'N-25º50'N based on data collected at moorings and from AUV surveys (Düing and Johnson, 1971; Lee and Moore, 1977; Correa et al. 2012). The maximum speed of the countercurrent can sometimes exceed 50 cm/sec and the current can extend vertically about 200 m above the bottom. Submersible dives on the coral mounds at the foot of the terrace show that their steeper slopes and live coral colonies tend to occur on the northern slopes of the mounds (Correa et al. 2012). This is evidence of fairly persistent southerly currents as elsewhere in the Straits, the coral growth is on the current-facing south slopes of the mounds. Our model results, however, do not show such a persistent countercurrent. Rather, reverse currents on the western side of transient eddy occur frequently over a broad area between 400-700m and spanning 20-30 km in N-S distance. However, these earlier surveys are either relying on spatially sparse stations (Lee and Moore, 1977) or limited to small areas of AUV mapping or a few mooring stations. Thus while it is possible that the model missed producing this countercurrent, another possibility is that what they observed is the return currents along the west side of a cyclonic eddy.

3.4. Bottom DIC and TA distributions

Modeled variability of near bottom carbonate chemistry is closely associated with the physical processes, particularly upwelling of deep cold waters. In fact, the bottom DIC pattern largely mirrors bottom temperature, while bottom TA pattern largely follow temperature because of the nearly opposite relationships between TA and DIC to temperature in these waters, i.e.,

lower temperature corresponding to lower TA but higher DIC, within the range of the bottom temperature in these areas (8°C < T <16°C) (Figure 2b, c). We focus on bottom and cross-sectional DIC distributions on the Pourtalès Terrace and Miami Terrace during the same periods as shown in Figures 7-9 (Figures 10-11).

During normal situations without the presences of eddies, cold DIC-rich waters cover most of the Pourtalès Terrace, with the exception being the southeastern flank due to persistent upwelling noted above (Figure 10a, b). The passage of a mesoscale eddy clearly brings more deep water onto the terrace, increasing the spatial coverage of high DIC waters including flooding the southeastern part of the terrace (Figure 10e, f). After the eddy passes, downwelling brings warm and reduced DIC waters over western part of the terrace (Figure 10g, h). In the deeper areas (>400 m) where temperature is lower than 12°C, however, there is little change in DIC concentration over time and space (Figure 10, right panels). This is because within this temperature range (4-12°C) waters are within the salinity minimum zone (Figure 2a) and both DIC and TA concentrations are in the neighborhood of their local extrema with a narrow range of variations (<25 μmol/kg).

Over the Miami Terrace, bottom DIC concentrations are also closely associated with bottom temperature following the development of island wakes and the upwelling of deep cold waters (Figure 11). When the transient eddy is not present, upwelling is already strong and high DIC waters cover much of the terrace, but the outer edge of the platform is covered by relatively warmer water with lower DIC concentration (Figure 11a, b). When an eddy is formed in the wakes, strengthened upwelling brings up more cold DIC-rich waters and the entire terrace is flushed with high DIC waters (Figure 11c-f). Similarly, the downwelling after the passage of the eddy reduces the DIC concentrations over the much of the terrace (Figure 11g, h). Yet again,

there is little change (<10 μmol/kg) in DIC concentrations over the deeper areas (> 400m) where temperature is lower than 12°C (Figure 11, right panels).

3.5. Temporal variability of bottom water properties

In order to understand the temporal variability of bottom water properties, we chose four representative locations, one on the platform (160 m) and another on upper slope (296 m) (below the platform) of the Pourtalès Terrace, one on the platform (280 m) and another on the upper slope (417 m) of the Miami Terrace (Figure 1). The time-series of T, S, DIC and TA concentrations, and aragonite saturation at these locations are shown in Figure 12. The modeled results suggest somewhat larger ranges of temperature (8-17.9°C) on top of the platform than that (8.2-14.2°C) over the upper slope over the Pourtalès Terrace (Figure 12a, b). The salinity shows a similar range (35.1-35.8 psu) at both locations. It is interesting to note that bottom temperature on the platform of the Pourtalès Terrace is normally lower than that over the upper slope area throughout the modeling period, except during a few episodic events. Spatially, the warmer area generally covers the southeast part of the terrace between 200 m and 400 m isobaths (Figure 7a, c). A close examination indicates most of the events are due to the passage of mesoscale eddies, which first induce strong upwelling along the leading fronts to greatly reduce the bottom temperature over the upper slope (Figure 7c-f) and then drive strong downwelling along their trailing edges to greatly increase temperature on the platform (Figure 7g, h). The bottom temperature and salinity changes during these events can be up to 6°C and 0.6 psu, respectively, at both locations.

In comparison, both bottom temperature and salinity on the platform of the Miami Terrace also show strong temporal variability, with a temperature range of 6-14.5°C and a salinity range of 34.9-35.9 psu (Figure 12a, b). Overall, waters at this location are 2-4°C colder

and fresher than waters on both the platform and upper slope of Pourtalès Terrace, even though the water depth here is comparable to the upper slope site of Pourtalès Terrace, suggesting stronger impacts of upwelling due to the island wakes and associated eddies. At the deeper site (417 m), both temperature and salinity are very stable, showing little changes over time ($6^oC<T<9.7^oC$, $34.9<S<35.3$). Bottom temperature and salinity at the two sites on the Miami Terrace are quite similar, except during a few downwelling events when temperature and salinity on the platform increase up to 6°C and 0.75 psu and during a prolonged warm period 2012 from mid-August through the end of November. Those downwelling events typically last from a few days to more than 1 week, mostly due to the passage of transient eddies spun off from the island wakes.

The temporal variability of near bottom DIC and TA concentrations are also closely associated with water movements as seen in Figures 7-10 (Figure 12c, d). Both DIC and TA concentrations on the platform of Pourtalès Terrace show a wide range on short-term (~weekly), 2,140-2,210 μmol/kg for DIC and 2,305-2,360 μmol/kg for TA, respectively. In contrast, both DIC and TA show much narrower ranges, <30 μmol/kg, over the upper slope of the Pourtalès Terrace. Consistent with the variability of bottom temperature, bottom DIC/TA concentration on the platform is normally higher/lower than that over the upper slope area throughout the modeling period, except during a few episodic events such as when an eddy passes through the area. This is consistent with the spatial pattern seen in Figure 10a and 10c, which show that waters with relatively low DIC concentration covers much of the southeastern part of the terrace between 200 m and 400 m isobaths. Coincidently, this relatively low DIC area overlaps with most of the NOAA designated HAPC for the Pourtalès Terrace (e.g., Reed et al. 2013). On the platform of the Miami Terrace, DIC and TA concentrations show somewhat larger ranges

(45 μmol/kg for DIC and 35 μmol/kg for TA) than those on the upper slope of Pourtalès Terrace. On the upper slope of the Miami Terrace, both parameters are fairly stable with a narrow range <10 μmol/kg throughout the modeling period. In deep areas (> 400 m), bottom values of these two parameters are effectively constant throughout the Straits as shown in Figures 10-11.

A simply correlation analysis of these time-series indicates that temperature alone explains > 76% of low frequency variability in bottom DIC and TA in these areas, except for the upper slope of Miami Terrace (56% for both DIC and TA). For short-term (high frequency) variability, temperature explains >64% of DIC and TA short-term variability for the two sites on the platform of the Pourtalès Terrace and Miami Terrace (see Table 3). The correlations between high frequency T and DIC variability for the two upper slope sites of the terraces are either weak or non-existent, reflecting the low DIC range (<15 μmol/kg) for these water masses (Figure 2b). In contrast, the T-TA correlation for the high frequency variability remains strong (r=0.92) on the upper slope of the Pourtalès Terrace. However, it is significantly weaker at r=0.69 on the upper slope of the Miami Terrace.

We note that these ranges of temperature variations, particularly at those stations on top of the platforms of both terraces may be somewhat exaggerated. Based on the model-data comparisons at the T2 and T3 mooring stations and assuming the model performances over these two terraces are similar, we can roughly estimate the variability of bottom temperature (measured with the standard deviation) at the two stations on top of the platforms (PT-160m and MT-280m) are roughly over-predicted by 20-30%. However, we do not have data to gauge the performance of temperature simulation in deeper areas. Given the modeled temperature ranges are smaller in these areas, we shall expect less model biases from the modeled temperature at the two deeper stations (PT-296m and MT-417m). Both DIC and TA show nearly linear

relationships with the temperature within the modeled temperature ranges at the two stations on top of the platforms (PT-160m and MT-280m). Thus, the over-predictions of DIC and TA ranges at these two stations are likely similar to that of temperature, at 20-30%. In deeper areas (PT-296m and MT-417m), both the DIC and TA relationships with temperature are much weaker, within the temperature ranges (6-12°C) at these depths (see, e.g., Figure 2). Therefore, we shall expect the model over-prediction of DIC and TA ranges in these areas are likely small.

The temporal variability of T, DIC, and TA over the Pourtalès Terrace leads to significant variability in Ω_{Ar}, with the annual range between 1.2-2 (Figure 11e). On top of the Miami Terrace, Ω_{Ar} shows a similar pattern but with a smaller annual range, between 1.2-1.7. On the upper slope of the Pourtalès Terrace the Ω_{Ar} ranges 1.3-1.6, whereas on the upper slope of the Miami Terrace and all of the deeper area (>400 m) Ω_{Ar} is nearly constant, between 1.2-1.3 throughout the year. The narrow range of Ω_A for deep waters is associated with the narrow ranges of TA and DIC concentrations around the salinity minimum. Interestingly, Ω_{Ar} is also strongly correlated with temperature (r>0.81) for both low and high frequencies at all of the sites except for the upper slope site of the Miami Terrace, where the correlation is strong at low frequency (r=0.74) but much weaker for high frequency (r=0.57) (Table 3). As noted above, the variability of the key variables (T, DIC, TA) for Ω_{Ar} is somewhat over-predicted. For the two shallower stations (PT-160m and MT-280m), assuming a 20% over-prediction of temperature, DIC and TA variability (measured as std, see Table 1), a simple calculation using CO2SYS (Lewis and Wallace, 1998; Van Heuven et al. 2011) suggests that the variability of Ω_{Ar} may have also been over-predicted by ~20%. For the two deeper stations (PT-296 m and MT-417 m), assuming a 10% over-prediction of temperature would mean <5% over-prediction of DIC and TA variability because the DIC-T and TA-T relationships are mostly flat for the temperature

ranges experienced at these stations (6-12°C). Therefore, we shall expect the predicted ranges of Ω_{Ar} at these stations are fairly close to the actual range because small change in temperature alone does not change Ω_{Ar} very much. In brief, variability of water masses over these terraces driven by meso-scale eddies and FC meandering are strongest during spring and fall of the model period, and their impacts on the Ω_{Ar} variability are significant for the areas on top of the terraces but likely small for deeper areas.

3.6. Bottom distribution of aragonite saturation state (Ω_{Ar})

To further understand the bottom carbonate chemistry in these deep coral habitats, we present the annual mean bottom Ω_{Ar} value and its standard deviation for 2012, which were computed based on the daily bottom Ω_{Ar} derived from bottom temperature, salinity, DIC and TA (Figure 13). The results for 2011 are very similar (not shown). Model results indicate dynamic upper slope regions including the platform and upper slope areas, where FC meandering, eddies, and associated upwelling/downwelling all contribute to the variability of bottom water properties, and relatively stable lower slope regions. On top of the platforms of both terraces (between approximately 200-400 m), Ω_{Ar} is typically higher than 1.4. Due to the presence of deep cold waters, Ω_{Ar} is relatively low over the inner platform of Pourtalès Terrace and southern Miami Terrace. In contrast, the Ω_{Ar} value over the southeastern part of Pourtalès Terrace and northern part of Miami Terrace is significantly higher. These are the areas less affected by upwelling driven by bottom Ekman transport and island wakes, as discussed above. On average, the slope regions for the two terraces experience low to moderate aragonite saturation, between 1.4 and 2 (Figure 12a). Consistent with the variability of bottom water properties, aragonite

saturation on the platforms of both terraces and over the upper slope (<400 m) regions shows much more variability than in deeper areas (Figure 13b).

4. Discussion

The modeled results indicate that the variability of bottom water properties including carbonate chemistry in the Florida Straits, particularly over the two deep coral habitats, is strongly affected by the movements of deep waters such as upwelling and downwelling. These upwelling and downwelling events are due to mesoscale processes and meandering of the Florida Current, and are also influenced by water properties in the source waters. In the following, we first discuss the bottom water masses in the Florida Straits, and then evaluate the respective roles of mesoscale eddies, large-scale transport, and biogeochemical processes in these variability.

4.1. Bottom water masses over the deep coral habitats

Water masses in the Florida Straits are ultimately derived from the Caribbean Current, which becomes the LC as it enters the GOM through Yucatan Channel (Rivas et al. 2005). The LC either flows directly into the Florida Straits or loops into the northern GOM. Its recirculation loop impinges on the Florida Shelf near the Dry Tortugas (Gordon, 1967) and becomes the FC in the southern Straits of Florida. Therefore, depending on the mode of the Loop Current, water properties in the FC may more closely resemble GOM waters or Caribbean waters. To date, there are no reported measurements for DIC and TA concentrations in the Caribbean waters. Thus, we assume that their values are similar to those observed in the northern GOM (Figure 14, also see Figure 2).

Based on the T-S diagrams for the GOMECC2 survey along the WFL and EFL transect and our modeled results at the four chosen sites over the two deep coral habitats, it is clear that

bottom waters over these habitats primarily comprise of two types of water masses: the North Atlantic central water (NACW) ($10^{o}C<T<16°C$, $35.2<S<36.4$) and the GOM Central Waters (GOMCW) ($6°C<T<10°C$, $34.9<S<35.3$) (Figure 14a). The GOMCW is lying beneath the NACW and its origin can be traced back to AAIW (Atkinson, 1983). In deeper (>400 m) areas, however, it seems that the water mass is primarily from the GOMCW. In both the GOM and the Straits, above the NACW, is the North Atlantic Salinity Maximum Water (SMW) (S>36), which is not present in the bottom waters over these coral habitats. These water properties are largely consistent with the water masses observed at the stations between 10-20°N along the WOCE A20 transect in summer 1997. However, salinity in the AAIW observed along A22 is about ~0.15 *psu* lower than that in GOMECC2 cruise, suggesting either change in the source waters or modification along the transit path from the western tropical Atlantic Ocean (within North Brazilian Current) through the Caribbean Seas.

The modeled TA and DIC concentrations over these deep coral habitats are largely consistent with those observed along the GOMECC2 WFL and EFL transects (Figure 14b, c). Modeled DIC concentration on the platform of Pourtales Terrace, however, is about 0-15 μmol/kg higher than those observed along the two GOMECC2 transects, suggesting local enrichment. Also, consistent with water mass changes between WOCE A22 transect and GOMECC2 observations noted above, the GOMCW has about the same DIC concentration, but ~5-10 μmol/kg higher TA concentrations.

The Loop Current penetrated deeply into the northern GOM during most of 2011-2012, except during summer-fall 2012, based on the satellite altimetry (https://www.aviso.altimetry.fr/en/my-aviso.html). Therefore, CO_2 concentrations in both NACW and AAIW are likely further increased as a result of remineralization of organic matter

from the GOM shelf waters (Wang et al. 2013; Wanninkhof et al. 2015). Once entering the Florida Straits, the waters are compressed upward as the current passes through the Straits due to the dramatic shoaling (>1000 m within a distance of <200 km) of bottom topography. The low temperature and high DIC NACW and AAIW waters are further steered upward over the slope of the left flank due to FC meandering and eddies while being transported through the straits as noted above. These explain the modeled results that bottom water masses over the upper portion of these coral habitats, despite being relatively shallow <400 m, are comprise primarily of NACW and AAIW, whereas bottom waters over the deep areas > 400 m are primarily from the AAIW (Figure 14).

Global models have suggested that the equatorial North Atlantic will experience shoaling of aragonite saturation horizon (ASH) in the future due to the ocean acidification (Orr et al. 2005; Orr, 2011). Higher CO_2 concentrations are present in the AAIW because high anthropogenic CO2 uptake in the Southern Ocean (Sabine et al. 2004; Gruber et al. 2019) contribute to ocean acidification in the Straights . Given the close correlation of bottom water properties in the Straits with the GOMCW and AAIW, ocean acidification will likely greatly shift the bottom carbonate chemistry in these areas including more frequent low aragonite saturation and will possibly breach the Ω_{Ar}=1 threshold. Moreover, a recent study indicates that the Atlantic meridional overturning circulation will provide a fast-track delivery of acidified cold waters through high latitude deep-water formation and subsequently spreading over the deep oceans (Perez et al. 2018). This implies that the deep coral reefs in our study region may experience more stress due to the lower availability of carbonate ions. However, potential impacts of lowering Ω_{Ar} on deep corals remains poorly understood (e.g., Hoegh-Guldberg et al. 2017). So far, there are only limited direct experiments testing the effects of ocean acidification,

mostly focusing on calcification rates, and these results are mixed (e.g., Maier et al. 2009, 2012; Form and Riebsell, 2012; Lunden et al. 2014; Georgian et al. 2016a). Low Ω_{Ar} may also affect other aspects of deep corals including reproduction, larval growth and dissolution of dead skeleton. Yet, the exact effects of these are largely unknown.

Warming temperature, and deoxygenation are also expected as a result of global warming (Lunden et al. 2014), both of which will potentially add to the stress to deep corals. Global warming may also lead to a reduction in the volume transport of Florida Current as a result of the weakening north Atlantic meridional overturning circulation (Caesar et al. 2018). This could potentially lead to weaker interactions between Florida Current and the bathymetry, and the nonlinear instability, both in turn likely lead to reduced upwelling and less vigorous mesoscale activity. It is not immediately clear how increased vertical stratification of Florida Current may affect upwelling or mesoscale processes.

4.2. Mesoscale eddies versus large-scale processes

Several processes are involved in the current- and eddy-topography interactions and deep water transport over the Pourtalès and Miami Terraces. All of these processes are operating on the background of persistent upwelling due to bottom Ekman transport (Hsueh and O'Brien, 1976; Garrett et al. 1993; Weisberg and He, 2003; Roughan and Middleton, 2004) and also topographic steering due to the alongshore changes of bottom topography (e.g., Janowitz and Pietrafesa, 1982; Gula et al. 2015a, b). Furthermore, much of this also depends on the position and orientation of the Florida Current. Kourafalou and Kang (2012) suggested that eddy formation in the southern Florida Straits is strongly tied to the latitudinal position of the Florida Current. Over the Miami Terrace, our modeled results suggest that the dominant mesoscale process is the island wakes and associated transient eddy production. The island wakes and eddy

formation, however, are also likely largely modulated by the meandering and strength of Florida Current. Taken together, these results indicate the importance of large-scale processes in modulating bottom water properties over these deep coral habitats.

The relative effects of large-scale processes and eddies in driving the upwelling or cross-shelf transport, however, have not been quantified. Here, we explore this quantitatively through a correlation analysis between the bottom temperature and relative vorticity (at mid-depths) on the Pourtalès Terrace and Miami Terrace (Figure 15). Here we show the results for the two upper slope sites. The results for the shallower sites are similar, but more complicated due to transport of upwelled waters from upstream. We used a Lanczos low-passed filter to split the variability of these two parameters into high-frequency (<11 days), which is assumed to be due to mesoscale processes the most significant of which is eddies, and low-frequency (>11 days), which is largely due to the variability of the Florida Current position and transport. An 11-day cut-off is a somewhat arbitrary choice as the time-scale separating the low and high frequency. This kind of partition is commonly used, but does not completely isolate mesoscale effects because the FC meandering may indirectly affect mesoscale activities or vice versa (Kourafalou and Kang, 2012). It is worth noting that a previous study indicated that the Florida Current meandering has two dominant periods, 5 and 12 days (Johns and Schott, 1987) in the northern Florida Straits. Meinen et al. (2010) indicated that significant energy for the variability of FC transport lies within the periods of <10 days. A longer cut-off time, e.g., 15-day, does not significantly affect the results of our analysis below (see Figure S3).

It is clear that both low frequency FC variability and mesoscale processes contribute positively (negative correlation) to the upwelling of cold waters onto the Pourtalès Terrace. The FC meandering, however, shows somewhat stronger impacts than the eddies on the bottom

temperature variability (r=-0.59 versus r=-0.39, respectively). By contrast, the upwelling over the Miami Terrace is positively correlated to the relative vorticity (the longitudinal position), i.e., when the current core moves closer to the terrace (higher relative vorticity) the near bottom temperature is higher, and vice versa (r=0.57). Similar influences on temperature anomaly come from short-term processes due to the effects of island wakes and the transient eddy (positive correlation r=0.58). More specifically, high anomaly of relative vorticity (positive anomaly) indicates that the FC is close to the slope and that there is a lack of wakes associated with the positive temperature anomaly (a lack of upwelling). On the contrary, negative vorticity anomaly indicates a well-developed island wake, or the presence of the transient eddy, associated with strong upwelling (negative temperature anomaly).

These results suggest the important roles of both local physical processes and remote forcing on the bottom carbonate chemistry, which is strongly correlated with the bottom temperature, particularly for the low frequency variability and/or areas over the platforms (Table 3). However, impacts become nonlinear when upwelling is strong and near bottom cold waters at the base of the slope are upwelled to mid-slope due to the nonlinear T-DIC and T-TA relationships at the low temperature end for AAIW (Figure 2). On the other hand, changes of water properties (T, S, TA, DIC) in the source areas, GOM or Caribbean Seas, will affect the bottom water properties in the Florida Straits. The impacts of these, however, are likely largely on the low frequency variability. There is a significant but weak correlation (r<0.6) between the bottom water temperature over both the habitats and subsurface temperature in the Gulf on the low frequency time-scale (>11 days), whereas no significant correlation is found for high frequency signals (not shown).

4.3. Contributions of biological export and remineralization to bottom carbonate chemistry

Biological processes including phytoplankton photosynthesis, remineralization of organic matter, and calcification could also contribute to the change of total CO_2 and alkalinity in the water column (see, e.g., Wanninkhof et al. 2015). Here we only consider the phytoplankton photosynthesis and remineralization, which would, respectively, decrease and increase DIC by 1 μmol/kg per μmol/kg uptake or remineralization. Assuming these processes follow a 6.625 C/N Redfield ratio for photosynthesis and remineralization, photosynthesis (remineralization) incorporating (releasing) nitrate would slightly increase (decrease) alkalinity by 1/6.625 μmol/kg per μmol/kg carbon change. Phytoplankton photosynthesis is low with phytoplankton biomass being typically <4 μmolC/l (chlorophyll <1 μg/l) due to the limitation of low dissolved inorganic nitrogen concentration in the upper layer (e.g., Llopiz, 2018; Figure S2). Therefore, the variability of this term is unlikely a major factor to the variability of water column DIC concentration. For near bottom waters over these deep coral reefs, there is no photosynthesis and only remineralization of organic carbon takes place. Our model results indicate that particulate organic carbon (POC) concentration in the deep waters is typically an order lower than the dissolve organic carbon (DOC) concentration (not shown). This is consistent with the observed POC concentrations in the upper 150 m along a cross-slope transect off Jacksonville, FL, about 100 mile north of our northern boundary during the July 2015 ECOA cruise, which indicate a range of 2-6 μmolC/kg ((https://www.nodc.noaa.gov/oads/data/0157080.xml). Therefore the overall contribution of POC remineralization to DIC is small. As for the DOC contribution, during the transit from the upstream boundary in the Gulf of Mexico to the southern Florida Straits, we shall expect an increase of DIC by,

$$\Delta DIC = r_{DOC} DOC * \Delta t, \quad (1)$$

where r_{DOC} is the remineralization rate and Δt is the transit time. The measured DOC concentration was at 40-60 μmol/kg along the EFL transect during the GOMECC-2 survey. Hansel et al. (2004) reported a similar range of 40-50 μmol/kg along the same transect during a survey in January-February, 1998. Leichter et al. (2007) surveyed several transects from the Keys to offshore up to 250 m water depth in September 11-19, 2003 and reported DOC concentrations between 40-55 μmol/kg for waters with temperature between 12-15°C. Therefore, it seems reasonable to assume that near bottom DOC concentration has a range of 40-50 μmol/kg. Our model results indicate that the near bottom DOC concentration in this area is ~30-40 μmol/kg (not shown), which is lower than the observed value. Based on our model, it takes about 5-10 days for GOM water to transit from the model GOM boundary to the Pourtalès and Miami Terrace area. We assume r_{DOC}=0.01-0.03 day^{-1} at 10^{o}C water temperature, which is lower than the 0.03 day^{-1} used in Fennel et al. (2006). Therefore, based on equation (1) and assuming DOC=40 μmol/kg, we shall expect an increase of DIC ~ 4-10 μmol/kg during the transit from the GOM. During the same transit period, a small, 1-2 μmol/kg, decrease in TA is expected.

We have not included the contributions of sediment fluxes to the near bottom DIC and alkalinity, which may be significant because of active sediment diagenesis and strong sediment transport due to the strong near bottom currents, up to 50 cm/sec, that these reefs experience. Strong currents are expected to be the main mechanism for sediment input from upstream. However, little is known regarding the related benthic biogeochemical processes.

5. Summary and Conclusions

A numerical model was developed to simulate the coupled physical-biogeochemical processes on the south Florida shelf and in the Florida Straits and a two-year (2011-2012) simulation was carried out. Built on previous work by Pan et al. (2017), we further gauge the model performance by comparing the model results with limited available data from two research cruises, transport measurements along 27°N, and several deployments of two ADCP moorings that took place during the model period. The results show overall agreement between model output and observations, including the magnitudes of high frequency (<11 days) variability in temperature, currents and FC volume transport. However, there are also discrepancies including over-predicting the magnitude of the temporal variability of water properties such as a temperature at the two mooring sites, over-estimating the bottom W-E velocity at the two mooring sites, and under-predicting the low frequency transport variability. One possible reason for these discrepancies is that the model does not fully capture the interactions of low frequency Rossby waves with the complex bathymetry in this area due to the model resolution. The model reproduces the general vertical structure of key parameters (T, S, TA and DIC) including the near permanent upwelling over the western slope along the 27°N transect observed during the GOMECC-2 survey.

Model results were then used to examine the spatial-temporal variability of key physical and carbonate chemistry parameters (temperature, salinity, DIC and TA) over the Pourtalès and Miami Terraces, two large deep coral reef habitats in the Florida Straits, and the associated mesoscale and large-scale processes. Four representative sites were chosen for an analysis of the temporal variability of bottom water properties over the two deep coral habitats. The results indicate that the near-bottom carbonate chemistry over both the Pourtalès and Miami Terraces is

strongly impacted by the meandering of the Florida Current and associated mesoscale eddies with differing effects in the two areas. As a general background, the Florida Current forces strong near-bottom upwelling over the Pourtalès Terrace resulting from bottom Ekman transport. As the current moves northward and gets closer to the slope, the bottom upwelling strengthens, and vice versa, as reflected in the negative correlation between bottom temperature and relative vorticity. Mesoscale eddies further enhance the upwelling by lifting up the thermocline along their leading front and eddy center. Together, these processes bring cold CO_2-rich but low-alkalinity deep waters onto the platform. The trailing edge of these eddies, however, drives significant downwelling, which leads to significantly warmer temperature and lower CO_2 concentration on top of the platform. Over the Miami Terrace, by contrast, island wakes behind the sharp topographic change and the frequent spin-off of the transient eddy over the Pourtalès Drift play a dominant role in driving the upwelling of CO_2-rich deep waters. The meandering and transport variability of the Florida Current together modulate the instability of island wakes and the production of mesoscale eddies at the southern end of the terrace. Overall, stronger upwelling is seen when the Florida Current shifts eastward away from the slope leading to lower temperature and higher DIC concentration over to the upper slope and the platform. Previous studies suggest the presence of a persistent near bottom countercurrent between 400-700 m in this area. Our model results did not show this current. This is can be either that the model failed to reproduce this current or that the return flow (southward) is part (west side) of the spin-off eddy from the island wakes.

Modeled results suggest that the bottom water masses over the Pourtalès Terrace and upper Miami Terrace comprise largely of NACW and AAIW. As a result of the complex physical processes, however, bottom water properties (T, DIC, TA) on top of both the Pourtalès

Terrace and Miami Terrace exhibit strong temporal variability over weekly to monthly timescales with a significant range of aragonite saturation state (1.2-2.0). In contrast, deeper (>400 m) areas in the Florida Straits are flushed with AAIW and the bottom water properties are very stable within the neighborhood of the salinity minimum and with nearly constant aragonite saturation state between 1.2-1.3.

The bottom carbonate chemistry in the Straits is likely also significantly influenced by changes in the water properties in their sources (GOM or Caribbean) through large-scale transport and by the biogeochemical processes (remineralization of organic matter, sediment inputs) along the paths. Our estimate suggests that remineralization may further contribute to a DIC increase ~4-10 μmol/kg as waters transit from the GOM to the deep coral habitats. There is, however, significant uncertainty in this estimate, and it does not take into account the possible sediment fluxes of DIC and alkalinity along the transport paths, which depends on the mode of Loop Current and sediment diagenesis processes. Ocean acidification in the future will likely further reduce the pH and Ω_{Ar} leading to greater stress on the deep coral reef ecosystems in this region. However, here we did not directly examine the potential impacts of ocean acidification, which would require additional simulations incorporating the long-term ocean acidification effects, and is beyond the scope of this manuscript.

Acknowledgements: MJ is funded by the Harbor Branch Oceanographic Institute (HBOI) Foundation and Florida Atlantic University startup fund for this work. This is HBOI contribution #2265. The HYCOM model output was downloaded from https://hycom.org/data/gomu0pt04/expt-50pt1. We thank Dr. Chai at the University of Maine for providing the CoSINE model output. The data from the GOMECC cruises were obtained through

funds of the NOAA Ocean Acidification Program awarded to LB and RW. Cooperative Institute of Ocean Research, Exploration and Technology (CIOERT) at HBOI gratefully acknowledges funding provided by NOAA Office of Ocean Exploration and Research (OER Grant #: NA090AR4320073), NOAA Deep Sea Coral Research and Technology Program (DSCRTP; CIOERT Project #: II-CO-DCE-6), and NOAA Office of Marine and Aviation Operations (OMAO) in support of the research, ship time, and ROV time. The ADCP measurements used for this project were conducted by the Southeast National Marine Renewable Energy Center with support from the U.S. Department of Energy under award DE-EE0000319. Three anonymous reviewers provided thoughtful comments and suggestions that greatly improved the manuscript.

References

Anthony K.R.N, J.A. Maynard, G. Diaz-Pullido, P.J. Mumby, P.A. Marshall, L. Cao and O. Hoegh-Guldberg, 2011, Ocean acidification and warming will lower coral reef resilience. Global Change Biology 17:1798-1808.

Bellwood, D.R., T.P. Hughes, C. Folke, and M. Nystrom, 2004, Confronting the coral reef crisis. Nature 429(6,994), 827.

Büscher J.V., A.U. Form, and U. Riebesell U. 2017, Interactive effects of ocean acidification and warming on growth, fitness and survival of the cold-water coral Lophelia pertusa under different food availabilities. Frontiers in Marine Science 4:101, DOI 10.3389/fmars.2017.00101.

Caesar, L., S. Rahmstorf, A. Robinson, G. Feulner and V. Saba, 2018 Observed fingerprint of a weakening Atlantic Ocean overturning circulation, 556: 191-196, https://doi.org/10.1038/s41586-018-0006-5

Chassignet, E.P., Hurlburt, H.E., Metzger, E.J., Smedstad, O.M., Cummings, J.A., Halliwell, G.R., Bleck, R., Baraille, R., Wallcraft, A.J., Lozano, C., Tolman, H.L., Srinivasan, A., Hankin, S., Cornillon, P., Weisberg, R.H., Barth, A., He, R., Werner, F., Wilkin, J., 2009. US GODAE: global ocean prediction with the HYbrid Coordinate Ocean Model (HYCOM). Oceanography 22, 64-75. doi: 10.5670/oceanog.2009.39.

Cohen, A.L. and M. Holcomb, 2009, Why corals care about ocean acidification – uncovering the mechanism, Oceanography, 22, 118-127.

Correa, T. B. S., G. Eberli, M. Grasmueck, John Reed, A. Correa. 2012. Genesis and morphology of coldwater coral ridges in a unidirectional current regime. Marine Geology 326-328:14-27.

Dickson, A. G. 1990. Standard potential of the reaction: AgCl(s) + H2(g) = Ag(s) + HCl(aq), and the standard acidity constant of the ion HS04-in synthetic seawater from 273.15 to 318.15 K. Journal of Chemical Thermodynamics, 22:113-27.

Dong, C., J. C. Mcwilliams, and A. F. Shchepetkin, 2007, Island wakes in deep water, J. Phys. Oceanogr., 37: 962-981.

Düing, W. and D. Johnson, 1971, Southward Flow under the Florida Current, Science, 173 (3995), 428-430.

Fennel, K., J. Wilkin, J. Levin, J. Moisan, J. O'Reilly, and D. Haidvogel, 2006, Nitrogen cycling in the Middle Atlantic Bight: Results from a three-dimensional model and implications for the North Atlantic nitrogen budget, Global Biogeochem. Cycles, 20, GB3007, doi:10.1029/2005GB002456.

Fennel, K., J. Wilkin, M. Previdi, and R. Najjar, 2008, Denitrification effects on air-sea CO2 flux in the coastal ocean: Simulations for the northwest North Atlantic, Geophy. Res. Lett., L24608, doi:10.1029/2008GL036147.

Form, A. U., and U. Riebesell, 2012, Acclimation to ocean acidification during long-term CO_2 exposure in the cold-water coral Lophelia pertusa. Glob. Change Biol. 18, 843–853. doi: 10.1111/j.1365-2486.2011.02583.x.

Fratantoni, P.S., Lee, T.N., Podesta, G.P., Muller-Karger, F., 1998. The influence of Loop current perturbations on the formation and evolution of Tortugas eddies in the southern Straits of Florida. J. Geophys. Res., 103(C11), 24,759-24,799.

Garcia, R. F., and C. S. Meinen, Accuracy of Florida Current volume transport measurements at 27°N using multiple observational techniques, J. Atmos. Ocean. Tech., 31 (5), 1169-1180, doi:10.1175/JTECH-D-13-00148.1, 2014.

Garrett, C., P. MacCready, and P. Rhines, 1993, Boundary mixing and arrested Ekman layers: Rotating stratified flow near a sloping boundary. Annu. Rev. Fluid Mech., 25, 291–323.

Geider, R. J., H. L. McIntyre, and T. M. Kana (1997), Dynamic model of phytoplankton growth and acclimation: Responses of the balanced growth rate and the chlorophyll a: Carbon ratio to light, nutrient-limitation and temperature, Mar. Ecol. Prog. Ser., 148, 187– 200.

Georgian S.E., D. Deleo, A. Durkin, C.E. Gómez, M. Kurman, J.J. Lunden, and E.E. Cordes, 2016b. Oceanographic patterns and carbonate chemistry in the vicinity of cold-water coral reefs in the Gulf of Mexico: implications for resilience in a changing ocean. Limnology and Oceanography 61:648_665 DOI 10.1002/lno.10242.

Georgian S.E., S. Dupont, M. Kurman, A. Butler, S.M. Strömberg, A.I. Larsson, and E.E. Cordes, 2016a, Biogeographic variability in the physiological response of the coldwater coral Lophelia pertusa to ocean acidification. Marine Ecology 37:1345_1359. DOI 10.1111/maec.12373.

Gordon, A.L., 1967, Circulation of the Caribbean Sea. *Journal of Geophysical Research*, 72, 6207-6223.

Gruber, N., et al. (2019), The oceanic sink for anthropogenic CO2; from 1994 to 2007, *Science*, *363*(6432), 1193, doi:10.1126/science.aau5153.

Haidvogel, D. B. and A. Beckmann, 1999, Numerical ocean circulation modeling, Imperial College Press, London, 344 p.

Hoegh-Guldberg O., E.S. Poloczanska, W. Skirving, and S. Dove S, 2017, Coral Reef Ecosystems under Climate Change and Ocean Acidification. Front. Mar. Sci. 4:158. doi: 10.3389/fmars.2017.00158

Hsueh, Y. and J. J. O'Brien, 1971, Steady coastal upwelling induced by an along-shore current, J. Phys. Oceanogr., 1: 180-186.

IPCC, 2013, Climate Change 2013: The Physical Science Basis. Contribution of Working Group I to the Fifth Assessment Report of the Intergovernmental Panel on Climate Change, Stocker, T.F., D. Qin, G.-K. Plattner, M. Tignor, S.K. Allen, J. Boschung, A. Nauels, Y. Xia, V. Bex and P.M. Midgley (eds.), Cambridge University Press, Cambridge, United Kingdom and New York, NY, USA, 1535 pp.

Janowitz, G.S., and L. J., Pietrafesa, 1982. The effects of alongshore variation in bottom topography on a boundary current, or, topographically induced upwelling. *Cont. Shelf Res*. 1(2), 123–141.

Johns, W.E. and F. Schott, 1987, Meandering and transport variations of the Florida Current, *J. Phys. Oceanogr.*, 17 (8), 1128-1147.

Kang, D. and E. N. Curchitser, 2013, Gulf Stream eddy characteristics in a high-resolution ocean model, J. Geophys. Res.-Oceans, C118: 4474–4487, doi:10.1002/jgrc.20318.

Kleypas J.A. and K.K. Yates, 2009, Coral reefs and ocean acidification. Oceanography 22(4):108-117.

Kourafalou, V.H., Kang, H., 2012. Florida Current meandering and evolution of cyclonic eddies along the Florida Keys Reef Tract: Are they interconnected? J. Geophys. Res. 117. doi: 10.1029/2011JC007383.

Lee, T.N., 1975, Florida Current spin-off eddies. Deep Sea Res., 22, 753-765.

Lee, T.N., K. Leaman, E. Williams, T. Berger, and L. Atkinson, 1995. Florida Current meanders and gyre formation in the southern Straits of Florida. J. Geophys. Res. 100, 8607–8620. doi: 10.1029/94JC02795.

Lee, T.N., and D. Mayer, 1977, Low-frequency current variability and spin-off eddies on the shelf off southeast Florida. J. Mar. Res., 35, 193-200.

Lee, T.N. and C.N.K. Mooers, 1977, Near-bottom temperature and current variability over the Miami slope and terrace, Bulletin of Marine Science, 27(4): 758-775.

Leichter, J.J. et al. 2007, Nitrogen and oxygen isotopic signatures of subsurface nitrate seaward of the Florida Keys reef tract, Limnol. Oceanogr., 52(3), 1258–1267.

Le Hénaff, M., Kourafalou, V. H., Morel, Y., Srinivasan, A., 2012. Simulating the dynamics and intensification of cyclonic Loop Current Frontal Eddies in the Gulf of Mexico, J. Geophys. Res. 117. doi:10.1029/2011JC007279.

Lewis, E, and DWR, Wallace, 1998, Program Developed for CO2 System Calculations. ORNL/CDIAC-105. Carbon Dioxide Information Analysis Center, Oak Ridge National Laboratory, U.S. Department of Energy, Oak Ridge, Tennessee. doi:10.3334/CDIAC/otg.CO2SYS_DOS_CDIAC105.

Llopiz, J.K., 2008, The Trophic Ecologies of Larval Billfishes, Tunas, and Coral Reef Fishes in the Straits of Florida: Piscivory, Selectivity, and Niche Separation, Ph.D thesis, University of Miami. 177pp.

Lunden J.J., S.E. Georgian, and E.E. Cordes, 2013, Aragonite saturation states at cold-water coral reefs structured by Lophelia pertusa in the northern Gulf of Mexico. Limnology and Oceanography 58(1): 354_362, DOI 10.4319/lo.2013.58.1.0354.

Lunden J.J., C.G. McNicholl, C.R. Sears, C.L. Morrison, and E.E. Cordes, 2014. Acute survivorship of the deep-sea coral *Lophelia pertusa* from the Gulf of Mexico under acidification, warming, and deoxygenation. Frontiers in Marine Science 1:78 DOI 10.3389/fmars.2014.00078.

Machado, P.M., J. H. VanZwieten and I. Pinos, 2016, A Measurement-Based Analysis of the Hydrokinetic Energy in the Gulf Stream, Journal of Ocean and Wind Energy, 3(1), 25–30.

Maier, C., J. Hegeman, M.G. Weinbauer, and J. P. Gattuso, 2009, Calcification of the cold-water coral Lophelia pertusa under ambient and reduced pH.Biogeosciences 6, 1671–1680. doi: 10.5194/bg-6-1671-2009

Maier C., P. Watremez P, M. Taviani, M.G. Weinbauer, J-P. Gattuso, 2012, Calcification rates and the effect of ocean acidification on Mediterranean cold-water corals. Proceedings of the Royal Society B: Biological Sciences 279:1716_1723, DOI 10.1098/rspb.2011.1763.

Mehrbach, C., C. H. Culberson, J. E. Hawley, and R. M. Pytkowicz. 1973. Measurement of the apparent dissociation constants of carbonic acid in seawater at atmospheric pressure. Limnology and Oceanography, 18: 897-907.

Meinen, C. S., M.O. Baringer, and R. F. Garcia, Florida Current transport variability: An analysis of annual and longer-period signals, *Deep Sea Research I, 57, 835-846, doi:10.1016/j.dsr.2010.04.001, 2010.*

Mesinger, F., et al. 2006. North American Regional Reanalysis. Bull. Am. Meteorol. Soc. 87, 343-360. doi: 10.1175/bams-87-3-343.

Mienis, F. G.C.A. Duineveld, A. J. Davies, S.W. Ross, H. Seim, J. Bane, and T.C.E. van Weering, 2012, The influence of near-bed hydrodynamic conditions on cold-water corals in the Viosca Knoll area, Gulf of Mexico, Deep-Sea Res. I, 60, 32-45.

Mienis F., G. Duineveld, A.J. Davies, M. Lavaleye, S.W. Ross, H. Seim, J. Bane, H. van Haren, M. Bergman, H. de Haas, S. Brooke, and T. van Weering, 2014, Cold-water coral growth under extreme environmental conditions, the Cape Lookout area, NW Atlantic. Biogeosciences 11:2543-2560.

Mora, C., C.-L. Wei, A. Rollo, T. Amaro, A. R. Baco, et al. 2013, Biotic and Human Vulnerability to Projected Changes in Ocean Biogeochemistry over the 21st Century, PLoS Biology, 11(10): 1-14.

Orr, J. C., 2011, Recent and future changes in ocean carbonate chemistry. Ocean Acidification, J.-P. Gattuso, and L. Hansson (Eds.), Oxford University Press, p41-66.

Orr, J. C., et al. 2005, Anthropogenic ocean acidification over the twenty-first century and its impact on calcifying organisms. Nature, 437: 681-686.

Pan, C. et al. 2017, Modeling the impacts of the Loop Current on circulation and water properties over the Pulley Ridge region on the Southwest Florida shelf, Ocean Modeling, 112: 48-64.

Perez, F. F. et al. 2018, Meridional overturning circulation conveys fast acidification to the deep Atlantic Ocean, Nature, doi:10.1038/nature25493.

Pietrafesa, L. 1990, Upwelling processes associated with western boundary currents. In: Phosphate deposits of the world, neogene to modern phosphorites, Burnett WC, Riggs SR (eds), vol 3. Cambridge Univ. Press, Cambridge, pp 3–26.

Pitts P.A. and N.P. Smith, 1997, An Investigation of summer upwelling across central Florida's Atlantic coast: The case for wind stress forcing. Journal of Coastal Research, 13(1) 105-110.

Reed J.K., S. Farrington, A. David, C.G. Messing, D.E. Guzman, and S. Pomponi, 2012, NOAA CIOERT cruise report: survey of the deep-sea coral and sponge ecosystem of Pourtales Terrace, NOAA Ship Nancy Foster, Florida Shelf-Edge Exploration II (FLoSEE) Cruise, Leg 2 - September 23-30, 2011, NF-11-09-CIOERT. 130 pages.

Reed, J.K., S. Harter, S. Farrington, and A. David, 2014, Characterization and interrelationships of deepwater coral/sponge habitats and fish communities off Florida, USA. Chapter 5 in "Coral Habitat and Fish Interrelationships". CRC Press, p. 49-80.

Reed, J.K., C. Messing, B. Walker, S. Brooke, T. Correa, M. Brouwer, T. Udouj, and S. Farrington, 2013, Habitat characterization, distribution, and areal extent of deep-sea coral ecosystem habitat off Florida, southeastern United States. Journal of Caribbean Science 47: 13-30.

Reed, J.K., S. Pomponi, A. Wright, D. Weaver, and C. Paull. 2005, Deep-water sinkholes and bioherms of South Florida and Pourtales Terrace- Habitat and Fauna. Bulletin of Marine Science 77:267-296.

Reed, J.K., D. Weaver, S.A. Pomponi, 2006, Habitat and fauna of deep-water *Lophelia pertusa* coral reefs off the Southeastern USA: Blake Plateau, Straits of Florida, and Gulf of Mexico. Bulletin of Marine Science 78(2): 343-375.

Richardson, D.E. et al. 2009, Sailfish (*Istiophorus platypterus*) spawning and larval environment in a Florida Current frontal eddy, Progress in Oceanography, 82: 252–264.

Rivas, D. A. Badan, and J. Ochoa, et al. 2005, The Ventilation of the Deep Gulf of Mexico, J. Phys. Oceanogr., 35: 1763-1781.

Roberts, J.M., 2009, Cold-water coral reefs, in *Encyclopedia of Ocean Sciences*, J.H. Steele (Ed.), Academic Press, p615-625.

Roson, G., F. Rios, F. F. Perez, A. Lavın, and H. L. Bryden, 2003, Carbon distribution, fluxes, and budgets in the subtropical NorthAtlantic Ocean (24.5^{o}N), J. Geophys. Res-Oceans, 108, NO. C5, 3144, doi:10.1029/1999JC000047.

Ross S.W., S. Brooke, A. Quattrini, M. Rhode, J.C. Watterson, 2015, A deep-sea community at unusually shallow depths in the western North Atlantic Ocean off northeastern Florida. Marine Biology 162: 635-648

Ross, S.W. and M.S. Nizinski, 2007, State of Deep Coral Ecosystems in the U.S. Southeast Region: Cape Hatteras to southeastern Florida. p. 233-270, Ch 6, In: Lumsden, S.E., T.F. Hourigan, A.W. Bruckner and G. Dorr (eds.). The State of Deep Coral Ecosystems of the United States. NOAA Tech. Memo. CRCP-3. Silver Spring, MD. 365 pp.

Ross, S.W. and A.M. Quattrini. 2007. The Fish Fauna Associated with Deep Coral Banks off the Southeastern United States. Deep-Sea Research Part I 54: 975-1007.

Roughan, M., Middleton, J.H., 2004. On the East Australian current: variability, encroachment, and upwelling. J. Geophys. Res. 109, C07003. doi: 10.1029/ 20 03JC0 01833.

Sabine, C. L., et al. 2004, The Oceanic Sink for Anthropogenic CO_2, *Science*, *305*(5682), 367–371

Seim, H.E., D.P. Winkel, G. Gawarkiewicz, and M.C. Gregg, 1999, A Benthic Front in the Straits of Florida and Its Relationship to the Structure of the Florida Current, J. Phys. Oceanogr., 29, 3,125-3,132.

Shchepetkin, A.F., McWilliams, J.C., 2005. The regional oceanic modeling system (ROMS): a split-explicit, free-surface, topography-following-coordinate oceanic model. Ocean Modelling 9, 347-404. doi: 10.1016/j.ocemod.2004.08.002.

Smith, N., 1981, An investigation of seasonal upwelling along the Atlantic Coast of Florida. In: Ecohydrodynamics. J.C. Nihoul (ed), Elsevier, New York, pp79-98.

Soloviev, A. V., A. Hirons, C. Maingota, C. W. Dean, et al. 2017, Southward flow on the western flank of the Florida Current, Deep-Sea Res. I, 125: 94-105.

Stewart, A. L. and A. F. Thompson, 2015, Eddy-mediated transport of warm Circumpolar Deep Water across the Antarctic Shelf Break, Geophys. Res. Lett. 10.1002/2014GL062281.

Thresher, R.E., B. Tilbrook, S. Fallon3, N. C. Wilson, and J. Adkins, 2011, Effects of chronic low carbonate saturation levels on the distribution, growth and skeletal chemistry of deep-sea corals and other seamount megabenthos, Mar. Ecol. Prog. Ser., 442: 87–99, doi: 10.3354/meps09400.

Taylor, K.E., 2001, Summarizing multiple aspects of model performance in a single diagram. J. Geophys. Res., 106, 7183-7192.

Umlauf, L., H. Burchard, 2003: A generic length-scale equation for geophysical turbulence models, *J. Marine Res.*, 61, 235-265.

van Heuven, S., D. Pierrot, J.W.B. Rae, E. Lewis, and D.W.R. Wallace, 2011, MATLAB program developed for CO2system calculations, ORNL/CDIAC-105b, Carbon Dioxide Inf. Anal. Cent., Oak Ridge Natl. Lab., US DOE, Oak Ridge, Tenn..

Vinick C., A. Riccobono, C.G. Messing, B.K. Walker, J.K. Reed, and S. Farrington, 2012, Siting study for a hydrokinetic energy project located offshore southeastern Florida: protocols for survey methodology for offshore marine hydrokinetic energy projects, www.osti.gov/servlets/purl/1035555/, U. S. Department of Energy, vii + 93 pp.

Wang, Z.A., Wanninkhof, R., Cai, W.-J., Byrne, R.H., Hu, X., Peng, T.-H., Huang, W.-J., 2013. The marine inorganic carbon system along the Gulf of Mexico and Atlantic coasts of the United States: Insights from a transregional coastal carbon study. Limnol. Oceanogr. 58, 325-342. doi: 10.4319/lo.2013.58.1.0325.

Wanninkhof, R. 1992. Relationship between gas exchange and wind speed over the ocean. J. Geophys. Res. 97:7373–81

Wanninkhof, R., Barbero, L., Byrne, R., Cai, W.-J., Huang, W.-J., Zhang, J.-Z., Baringer, M., Langdon, C., 2015. Ocean acidification along the Gulf Coast and East Coast of the USA. Cont. Shelf Res. 98, 54-71. doi: 10.1016/j.csr.2015.02.008.

Weisberg R. H. and R. He, 2003, Local and deep-ocean forcing contributions to anomalous water properties on the West Florida Shelf, J. Geophys. Res 108 (C6), 3184, doi:10.1029/2002JC001407.

Xiu, P., and F. Chai, 2014, Connections between physical, optical and biogeochemical processes in the Pacific Ocean, Prog. Oceanogr., 122, 30–53.

Xu, X., W.J. Schmitz Jr., H. E. Hurlburt, and P. J. Hogan, 2012, Mean Atlantic meridional overturning circulation across 26.5°N from eddy-resolving simulations compared to observations, J. Geophys. Res.-Oceans, 117, C03042, doi: 10.1029/2011JC007586.

Yang, B., R. H. Byrne, and R. Wanninkhof, 2015, Subannual variability of total alkalinity distributions in the northeastern Gulf of Mexico, J. Geophys. Res-Oceans, 10.1002/2015JC010780.

Table 1. Changes of model parameters.		
Model parameters	**Fennel et al. (2006)**	**This study**
Light attenuation due to seawater (1/m)	0.04	0.025
PAR fraction of shortwave radiation	0.43	0.5
Inverse half-saturation for phytoplankton NO_3 uptake (1/μM)	2	1
Inverse half-saturation for phytoplankton NH_4 uptake (1/μM)	2	5
Phytoplankton natural mortality rate (day^{-1})	0.15	0.05
Maximum chlorophyll to carbon ratio (μgChl/μgC)	0.0535	0.04
Zooplankton grazing rate (day^{-1})	0.6	0.7
Half saturation constant for zooplankton grazing (μM)	2.0	0.2
Small detritus remineralization rate (day^{-1})	0.03	0.02
Phytoplankton sinking velocity (m/day)	0.1	1.0
Large detritus (PON) sinking velocity (m/day)	1.0	3.0

Table 2. Statistics for model-data comparison.

Dataset	Parameter	Label	RMSE	Point-to-point correlation*	Mean±STD		Mean difference (confidence interval)*
					Model	Data	
GOMEC2	Temperature (°C)	B	2.64	**0.93**	22.15±6.5	22.45±7.38	0.3
	Salinity (psu)	C	0.34	**0.65**	36.0±0.34	36.0±0.44	0
	DIC (μm/kg)	D	20.40	**0.96**	2093.3±71.0	2085.2±76.4	**8.1 (4.3-11.3)**
	TA (μm/kg)	E	18.40	**0.69**	2367.8±20.0	2357.8±25.2	**10.0 (6.7-13.9)**
	NO_3 (μm/kg)	F	4.50	**0.90**	6.89±8.58	8.17±10.2	**1.3 (0.6-2.0)**
	Chl (μg/l)**	G	0.15	**0.74**	0.15±0.17	0.14±0.16	0.005
FloSEE	Temperature (°C)	H	2.2	**0.97**	17.6±7.82	17.8±6.78	**0.25 (0.15-0.36)**
	Salinity (psu)	I	0.38	**0.75**	35.40±0.38	35.9±0.56	**0.47 (0.45-0.49)**
Moorings	T2 Temperature (°C)***	J	1.30	**0.23**	10.30±1.20	9.72±1.05	**0.5 (0.36-0.77)**
	T3 Temperature (°C)***	K	1.40	**0.27**	9.90±1.40	9.73±1.03	**0.2 (0.07-0.35)**
	U at B2, 78m (m/sec)	L	0.08	**0.23**	0.21±0.05	0.36±0.08	**0.16 (0.14-0.19)**
	V at B2, 78m (m/sec)	M	0.20	**0.66**	1.63±0.18	1.46±0.28	**0.16 (0.15-0.17)**
	U at B2, 156m (m/sec)	N	0.08	-0.04	0.16±0.03	0.29±0.09	**0.13 (0.11-0.14)**
	V at B2, 156m (m/sec)	O	0.18	**0.20**	1.17±0.14	1.05±0.14	**0.12 (0.10-0.14)**
Transport at 27°N	Volume (10^6 m^3/sec)	P	3.3	**0.19**	30.3±1.8	31.2±3.2	**0.91 (0.67-1.15)**

***** Unsigned difference. Bold values indicate significant correlation or mean difference at $p<0.01$. The mean difference (last column) was tested with the paired student-t test.

** Excluding points with modeled chlorophyll > 0.5 μg/l.

***Limited to low-pass (cutoff at 11-day) data, unsigned.

Table 3. Statistics of high and low frequency variability at the four stations.												
	STD high freq. (<11 day)				**STD low freq. (>11 day)**				**Correlation with temperature (low/high frequency)***			
	PT-160m	PT-296m	MT-280m	MT-417m	PT-160m	PT-296m	MT-280m	MT-417m	PT-160m	PT-296m	MT-280m	MT-417m
T	0.4	0.3	0.6	0.3	1.6	1.1	1.4	0.6				
S	0.03	0.03	0.06	0.03	0.15	0.14	0.16	0.06	**0.93/ 0.80**	**>0.98**	**>0.98**	**0.94/ 0.94**
DIC	4.1	1.7	3.2	1.0	13.0	4.1	6.8	1.1	**-0.94**/ **-0.88**	**-0.87**/ -0.36	**-0.93**/ **-0.80**	**-0.76**/ -0.09
TA	2.0	1.3	2.1	0.8	9.9	4.7	5.7	1.6	**0.94/ 0.86**	**0.96/ 0.92**	**0.98/ 0.92**	**0.76/ 0.69**
Ω_{Ar}	0.03	0.01	0.03	0.01	0.13	0.08	0.09	0.08	**0.97/ 0.96**	**0.94/ 0.81**	**0.97/ 0.90**	**0.74/ 0.57**

*Bold highlights the correlation coefficient greater than 0.5.

**Acronyms: PT – Pourtales Terrace, MT – Miami Terrace.

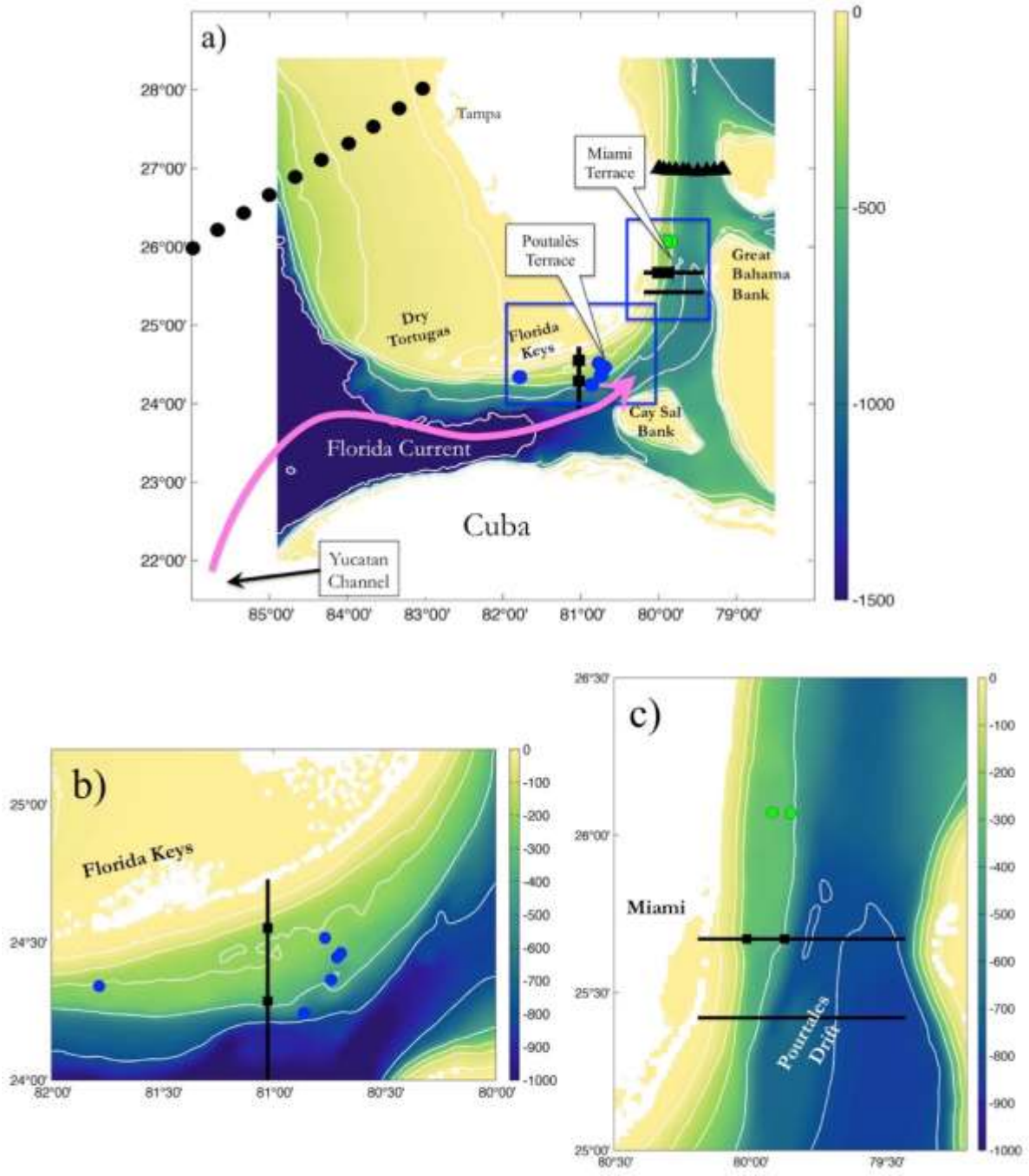

Figure 1. a) Model domain (delineated by the boundary of the bathymetry map) and bottom bathymetry, and b) and c) zoom-in maps for Pourtalès Terrace and Miami Terrace (see blue boxes in a)), respectively. White contours lines represent 20 m, 50 m, 100 m, 200 m, 400 m, 800 m and 1500 m. Also shown are sampling stations for GOMECC2 west Florida WFL (dots) and northern Florida Straits EFL (triangles) transects, NOAA FloSEE stations over the Pourtalès Terrace (blue dots), two SNMREC mooring stations T2 (316 m) and T3 (252 m) (green dots), and two transects (black lines) and four locations (squares) for model analysis. Note that the deeper stations along the GOMECC2 WFL transect were outside of the model domain. Also Loop Current is not shown in a).

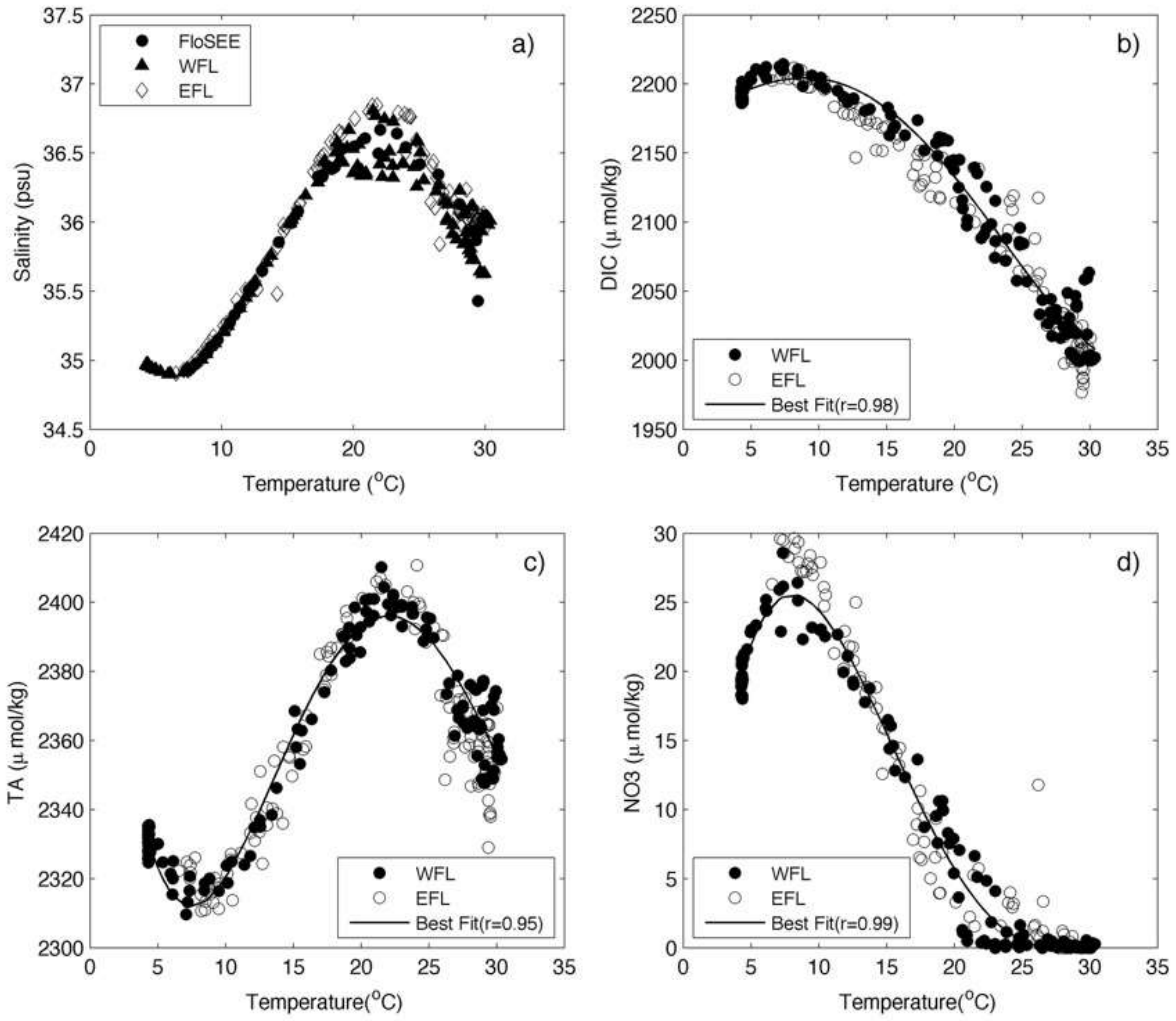

Figure 2. Temperature versus salinity, DIC, TA, and NO_3 along the GOMECC2 WFL and EFL transects: a) T-S (also plotted are data from FloSEE cruise), b) T-DIC, c) T-TA, and d) T-NO_3. Black lines in b)-d) represent the best polynomial fits for each pair for the data along the WFL transect.

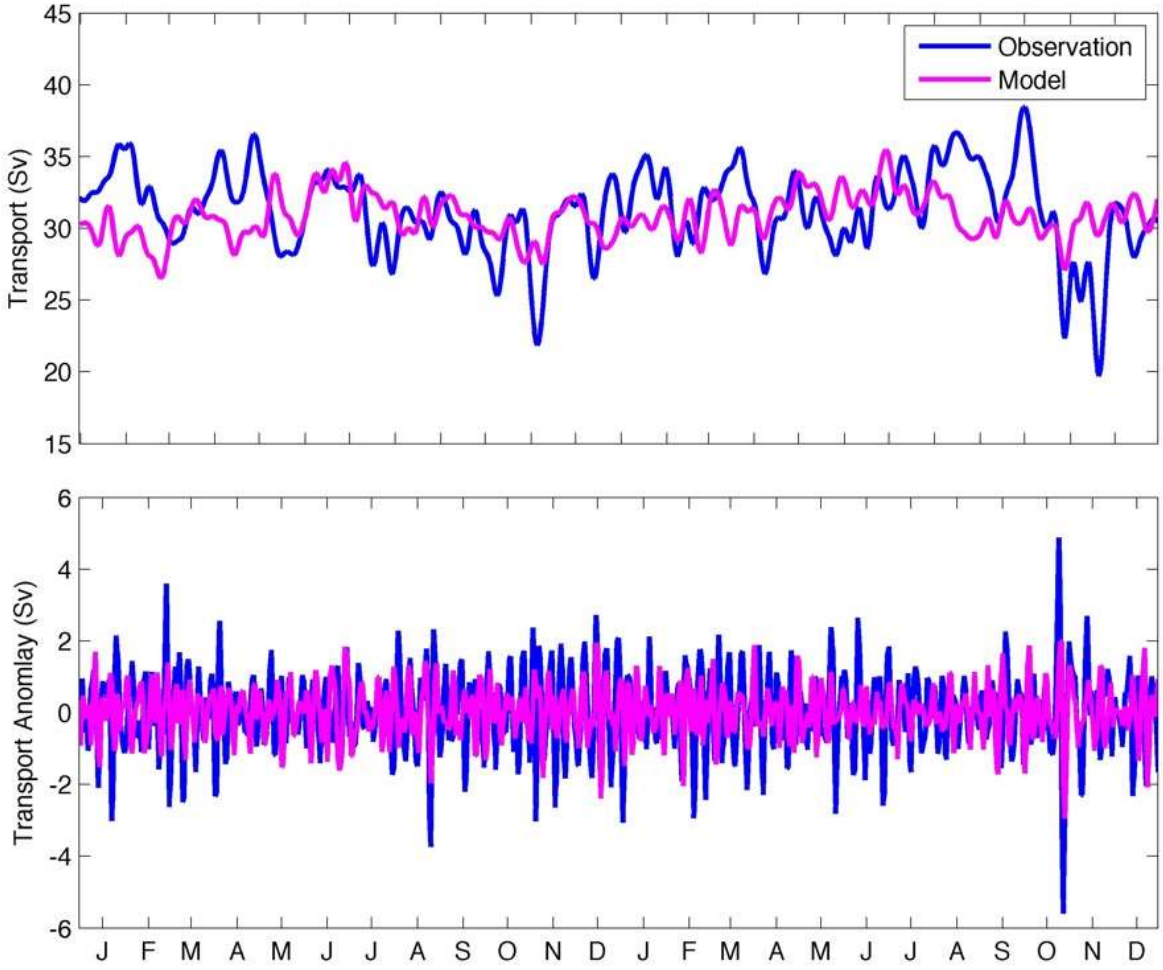

Figure 3. Model and observed integrated volume transport across 27°N: a) low-frequency (>11 day) and b) high-frequency (< 11 day) components.

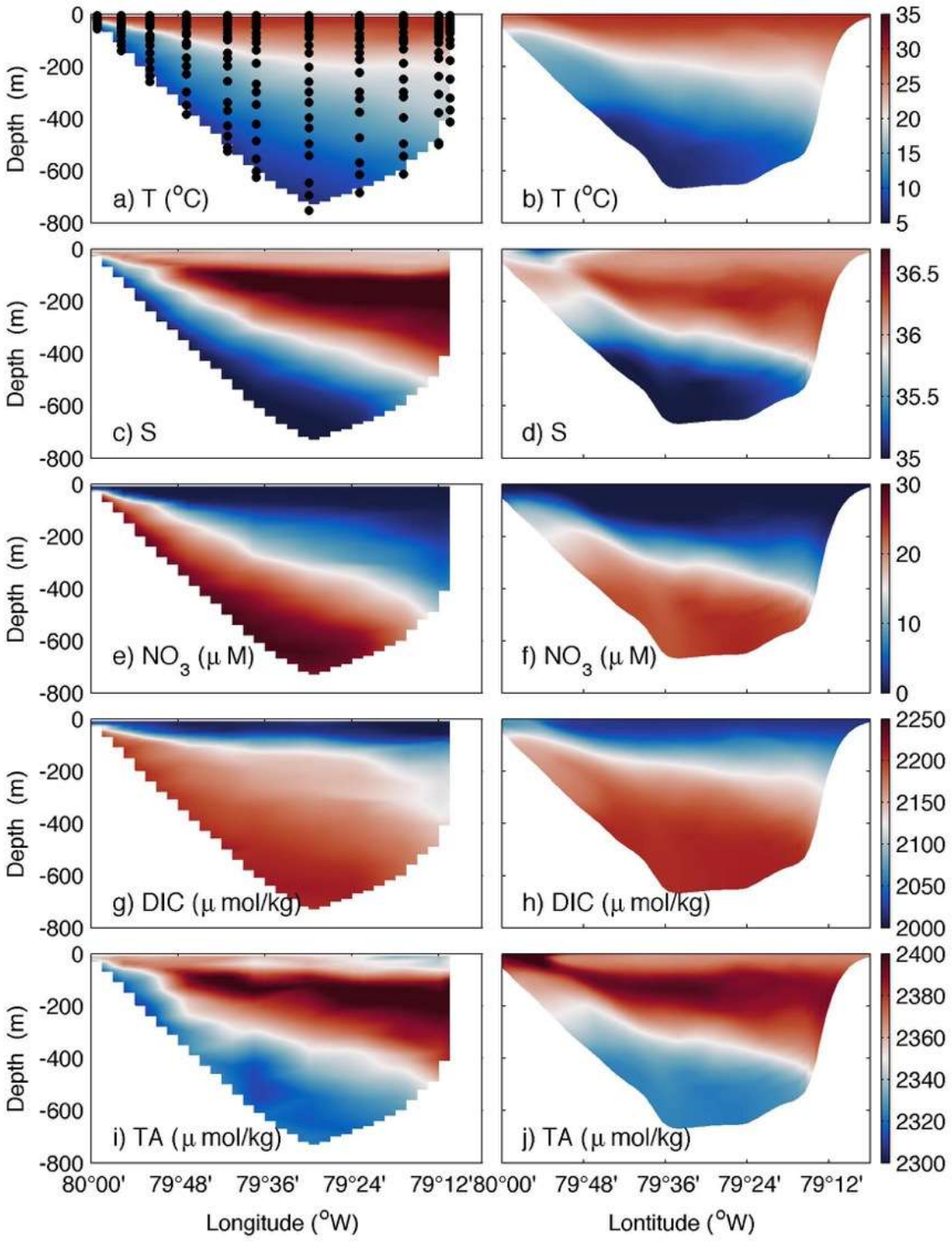

Figure 4. Observed (left panels) and modeled (right panels) temperature (a & b), salinity (c & d), nitrate (e & f), DIC (g & h) and TA (i & j) along the GOMECC2 EFL transect, which was surveyed in July 30-31, 2012. Modeled results shown are daily averages on July 31, 2012, when sampling for most of the GOMECC2 stations except the two at the shelf edge took place. Black dots in a) indicate the sampling depths.

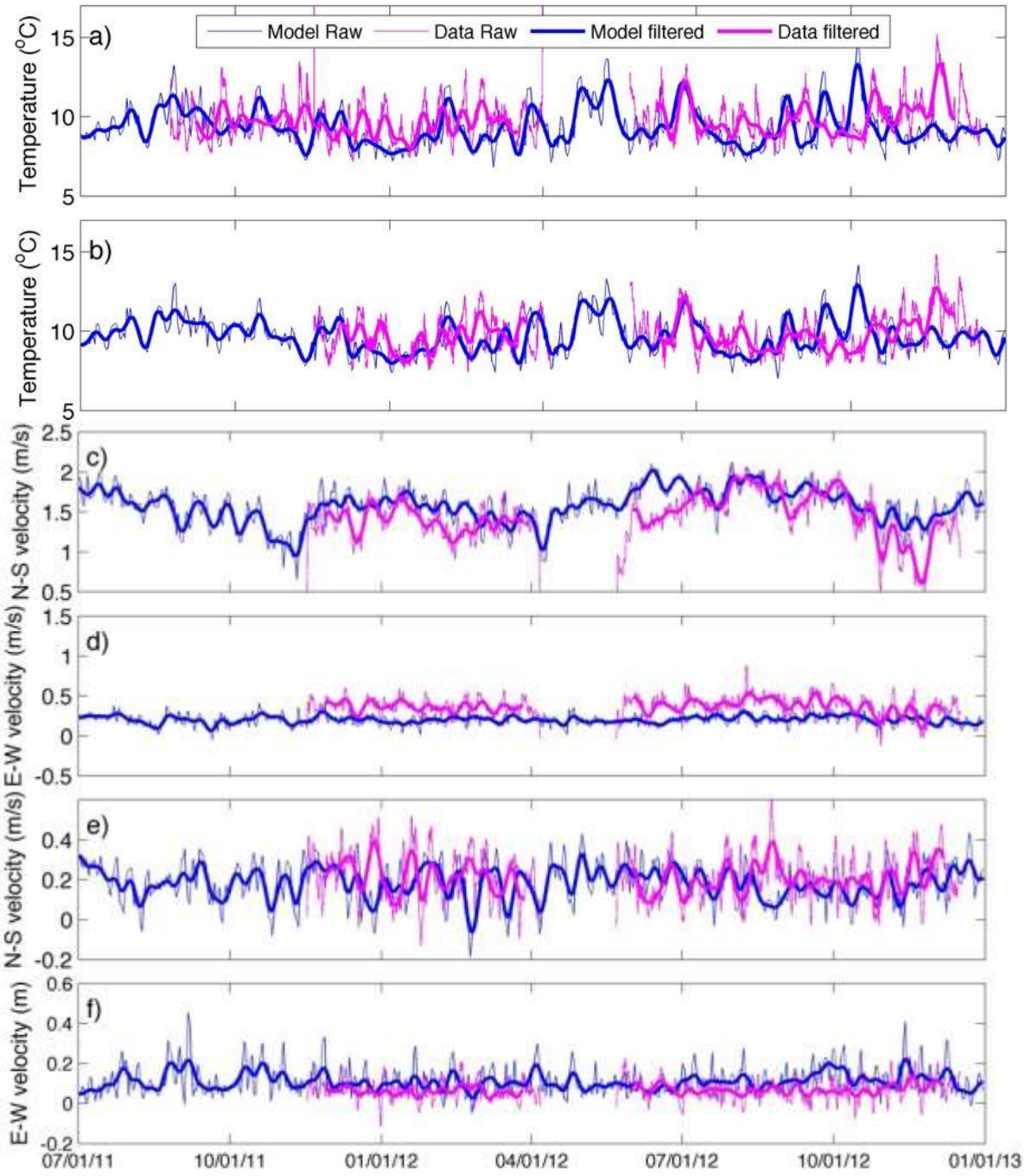

Figure 5. Model (blue lines) and observed (red lines) near bottom temperature and currents at the two moorings on the Miami Terrace: a) near bottom temperature at T3, b) near bottom temperature at T2, c) N-S velocity (78 m) at T2, d) W-E velocity (78 m) at T2, e) near bottom (17 mab) N-S velocity at T2, and f) near bottom (17 mab) W-E velocity T2. Bold solid lines are low-pass filtered with a Lanczos filter (11-day cut-off). For observed velocities, tidal signals were removed.

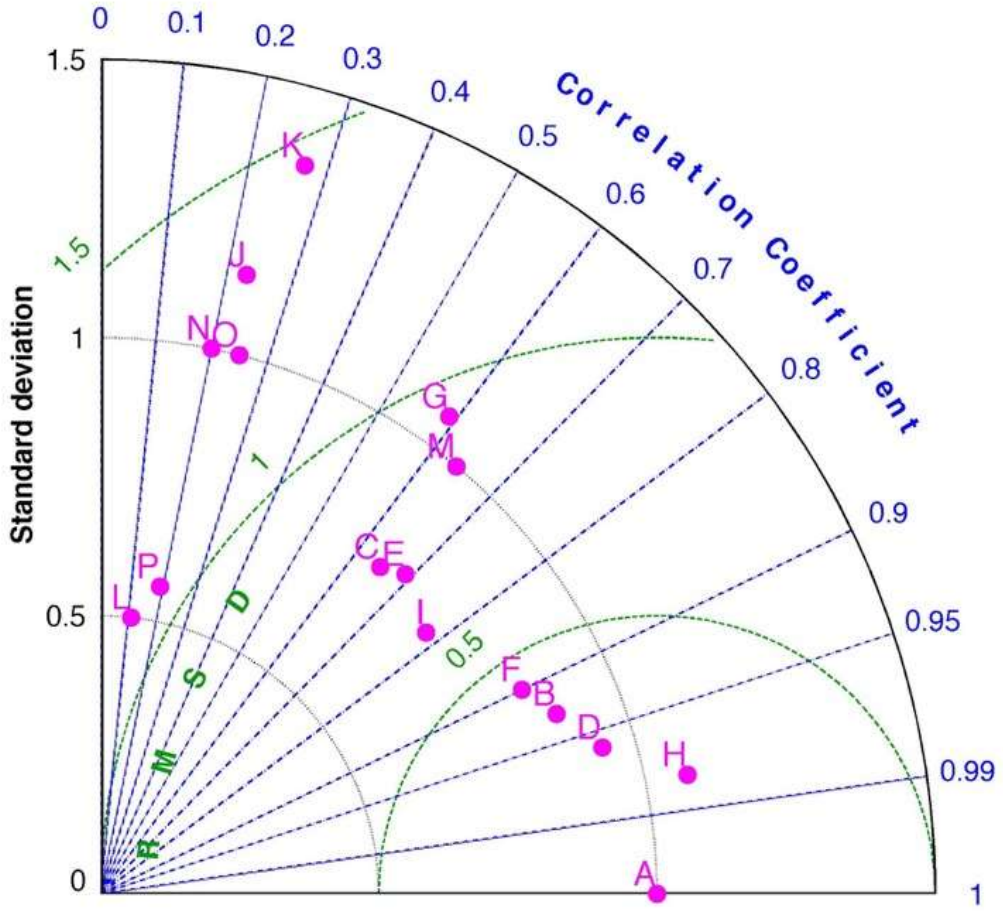

Figure 6. A Taylor diagram for model-data correlation, root mean square of errors (RMSE), and normalized standard deviation. A is the reference point for a perfect match between model and data and the rest of the letters are corresponding to the measurements listed in Table 2. All of the modeled standard deviations (stds) are normalized by the observed stds of the corresponding variables.

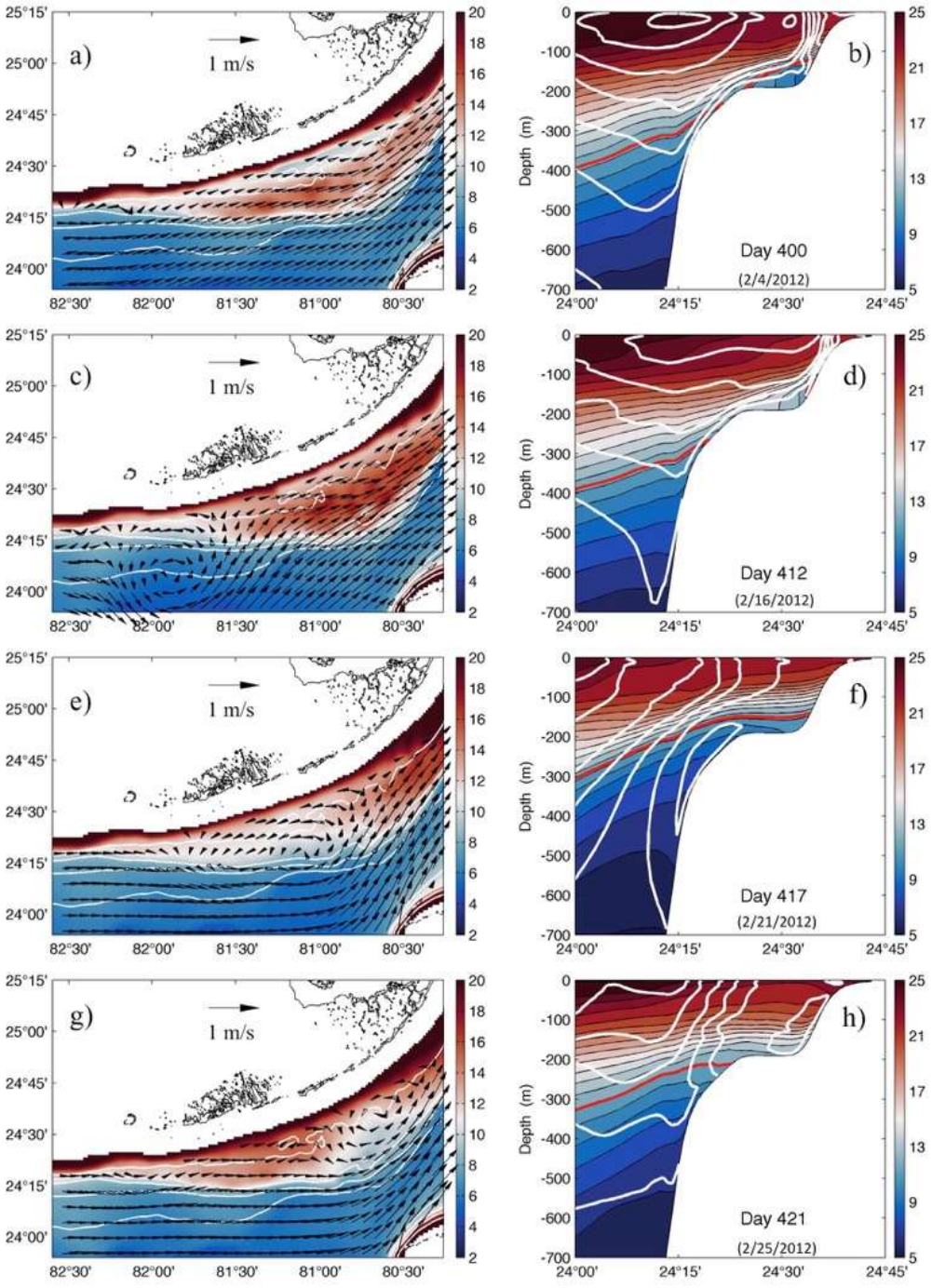

Figure 7. Left panels: Model bottom temperature (color) and 150 m currents (vectors) over Pourtalès Terrace. Red line indicates the N-S transect across the terrace. Blue dots indicate the two locations on the platform (160 m) and over the upper slope (296 m) of the terrace. White contours indicate the isobaths of 200 m, 400 m, 600 m, and 800 m. Right panels: Model temperature (color) and W-E velocity (while contour, interval=0.2 m/sec) along the 81^{o}W transect across the Pourtalès Terrace. Red line indicates the T=12^{o}C isotherm. Note the different color scales for temperature in left and right panels.

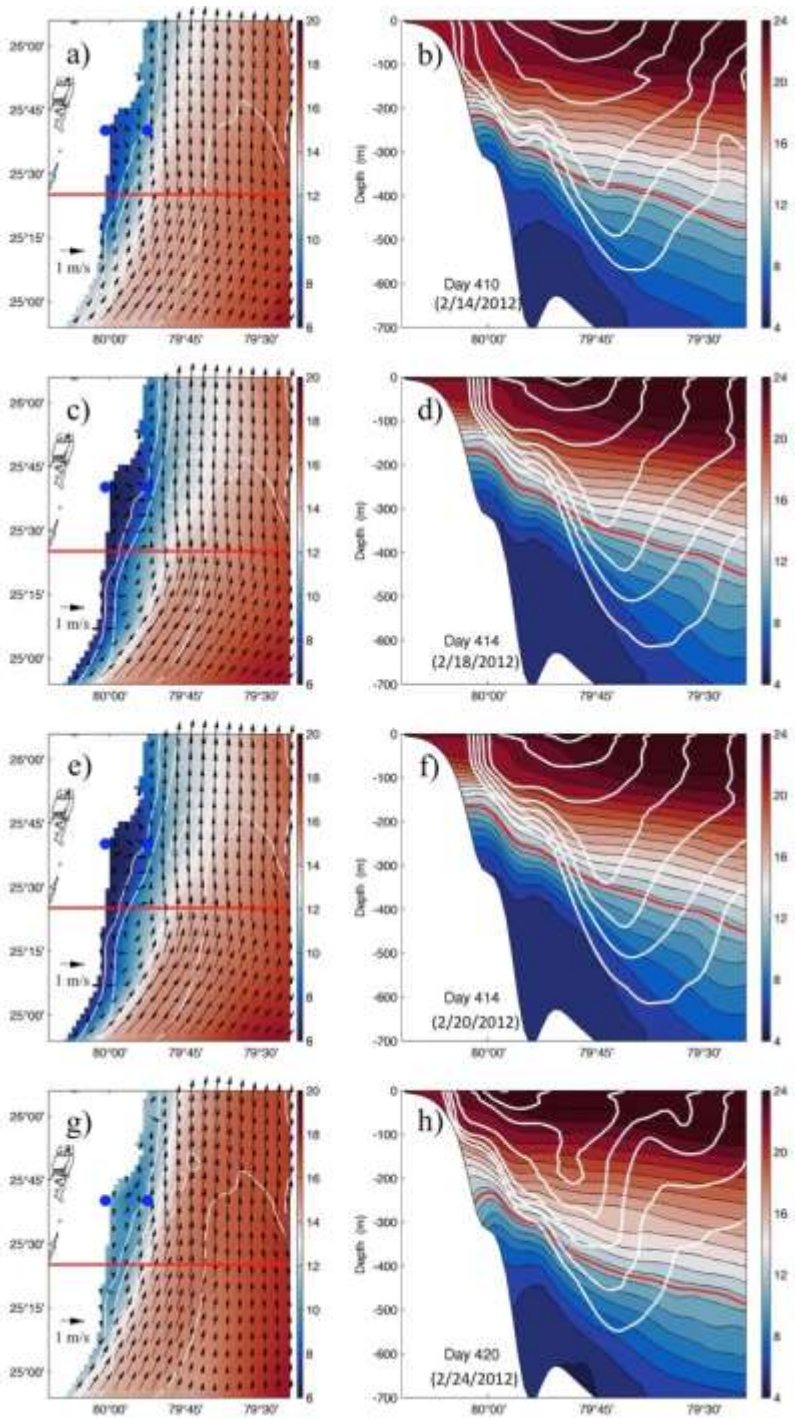

Figure 8. Left panels: Model 300m temperature (color) and currents (vectors) over the Miami Terrace. Red line indicates the cross-slope (W-E) transect (~25°25'N). White contours indicate the isobaths of 200 m, 400 m, 600 m, and 800 m. Blue dots indicate the two locations on the platform (280 m) and over the upper slope (417 m) of the terrace. Right panels: Model temperature (color) and N-S velocity (white contour, >0.6 m/sec only, interval=0.2 m/sec) along the cross-slope transect. Red line indicates the T=12°C isotherm. Note the different color scales for temperature in left and right panels.

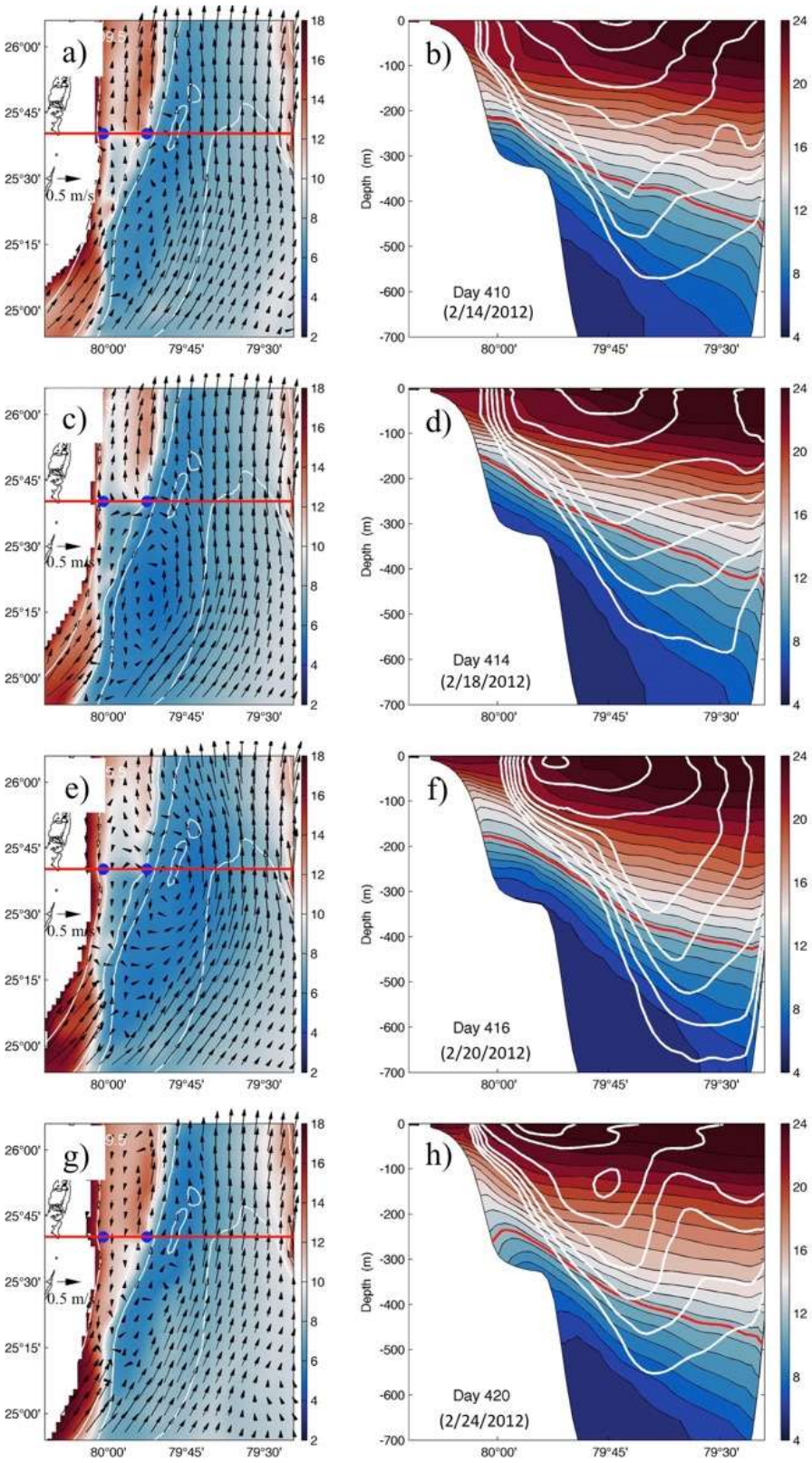

Figure 9. Same as Figure 8 except for bottom temperature (color) and currents (vectors) for left panels and the 25°40'N transect for the right panels.

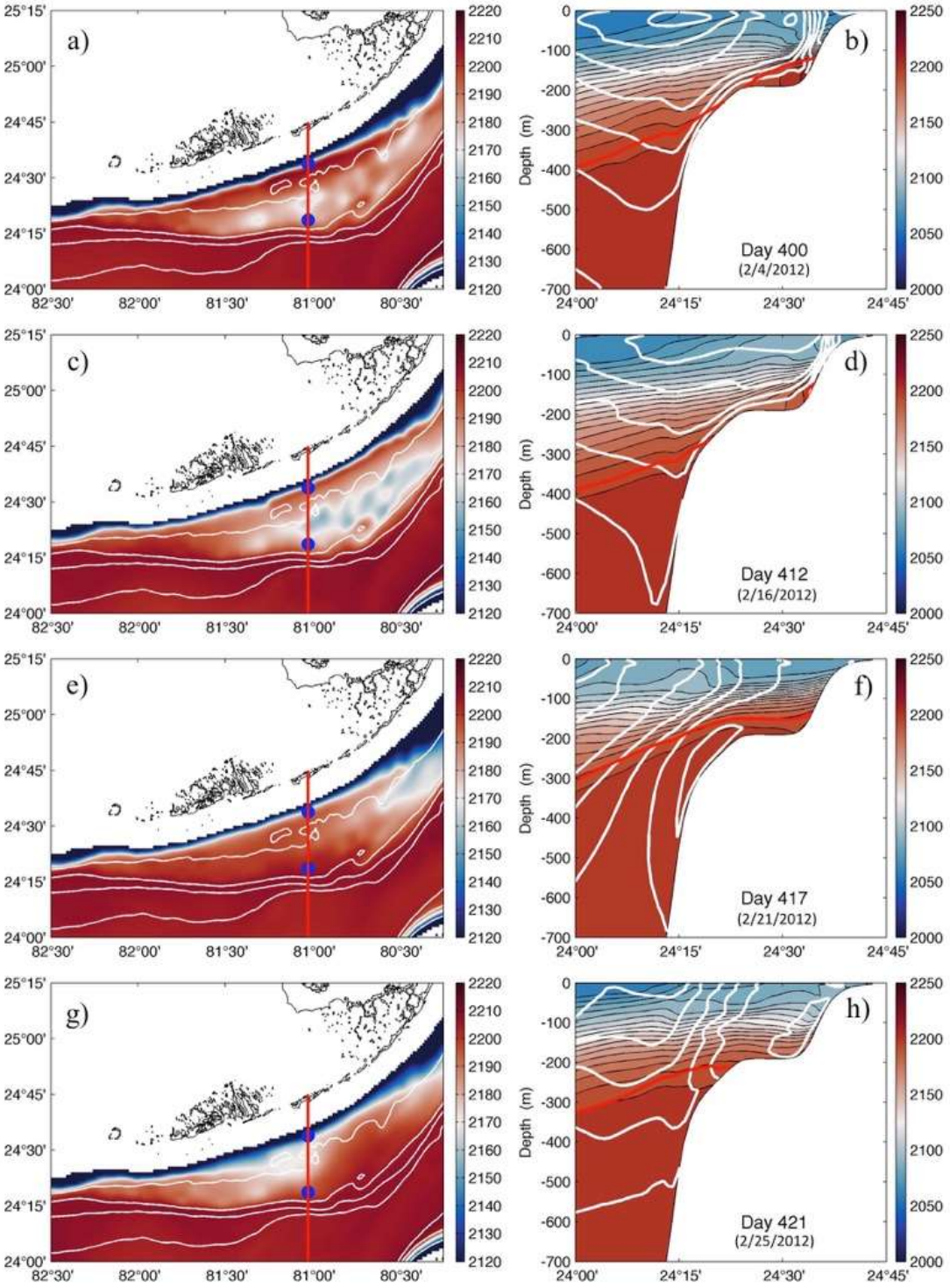

Figure 10. Same as Figure 7 but for bottom DIC concentration (left panels) and DIC (color) and W-E velocity (white contour) along the N-S transect (right panels). On the left panels, the red line indicates the N-S transect, and white contours indicate the isobars of 200 m, 400 m, 600 m, and 800 m. On the right panels, the red line indicates the T=12^{o}C isotherm. Note the different color scales for temperature in left and right panels.

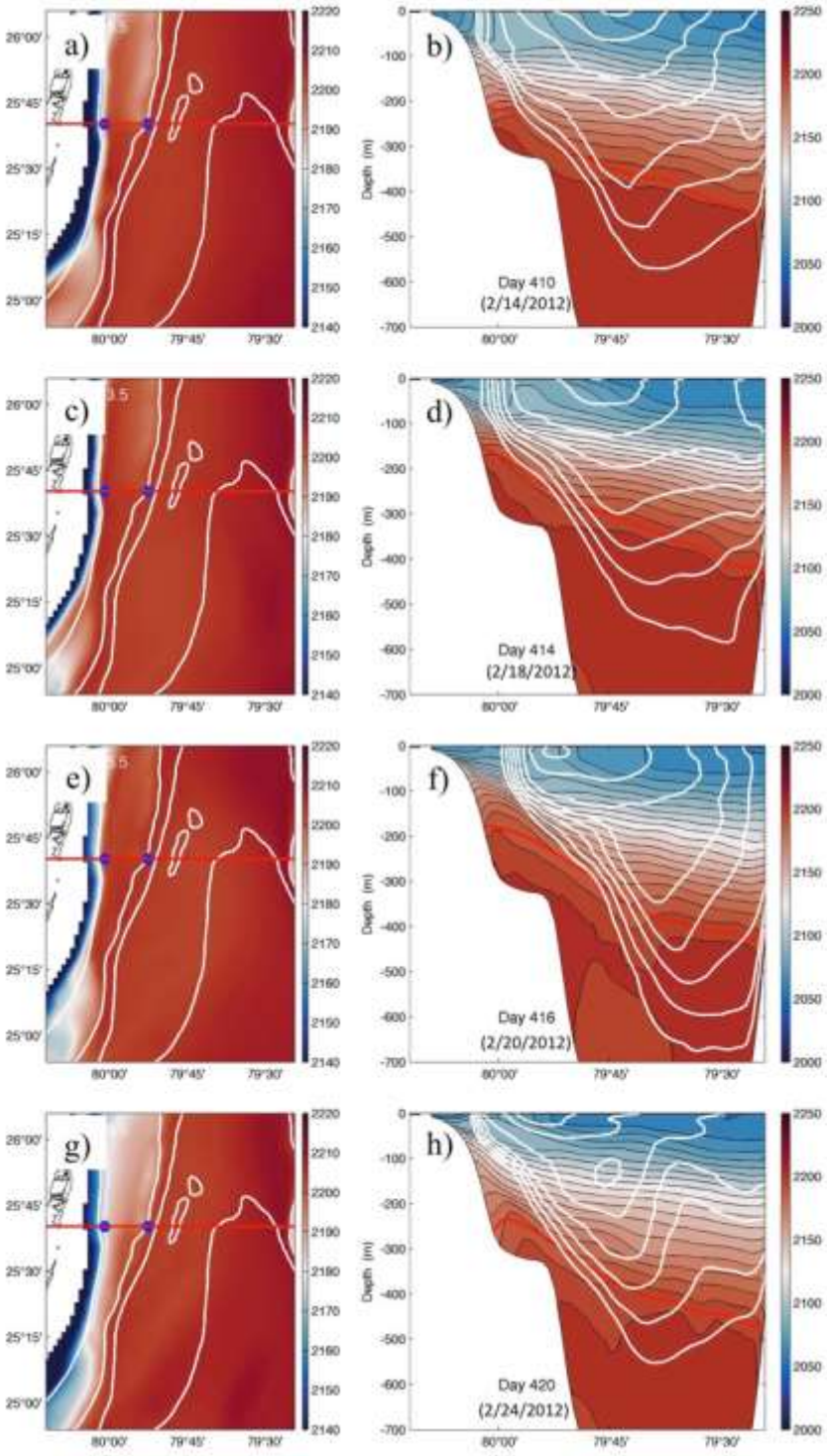

Figure 11. Same as Figure 8 but for model bottom DIC (left panels) and DIC (color) and N-S velocity (white contour) along the W-E transect (right panels). On the left panels, white contours indicate the isobars of 200 m, 400 m, 600 m, and 800 m, and the red line indicate the W-E transect. On the right panels, the red line indicates the T=12^{o}C isotherm. Note the different color scales for temperature in left and right panels.

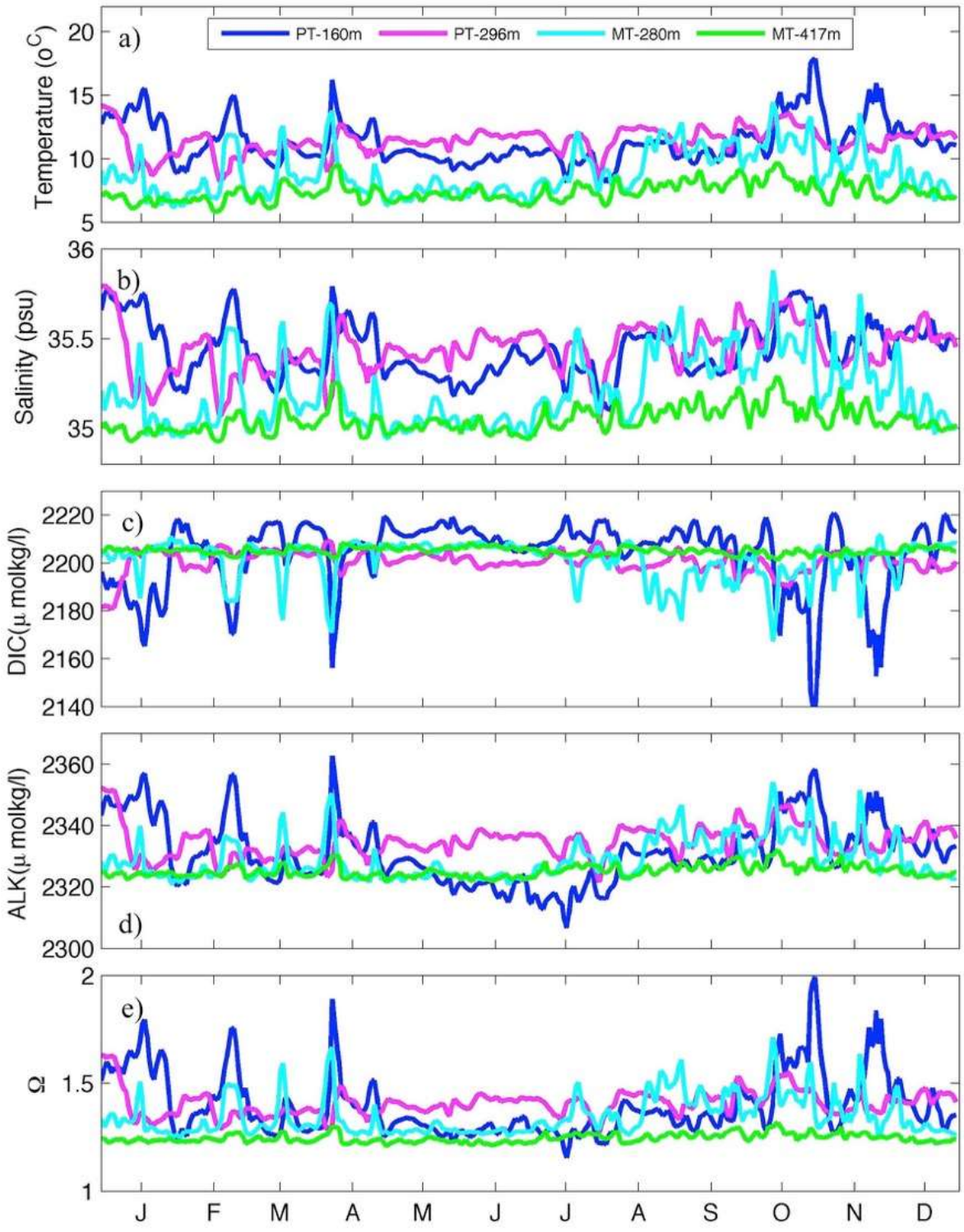

Figure 12. Model bottom temperature (a), salinity (b), DIC (c), TA (d), and aragonite saturation state (e) at the four chosen sites on Pourtalès and Miami Terraces (see Figure 1 for locations) in 2012.

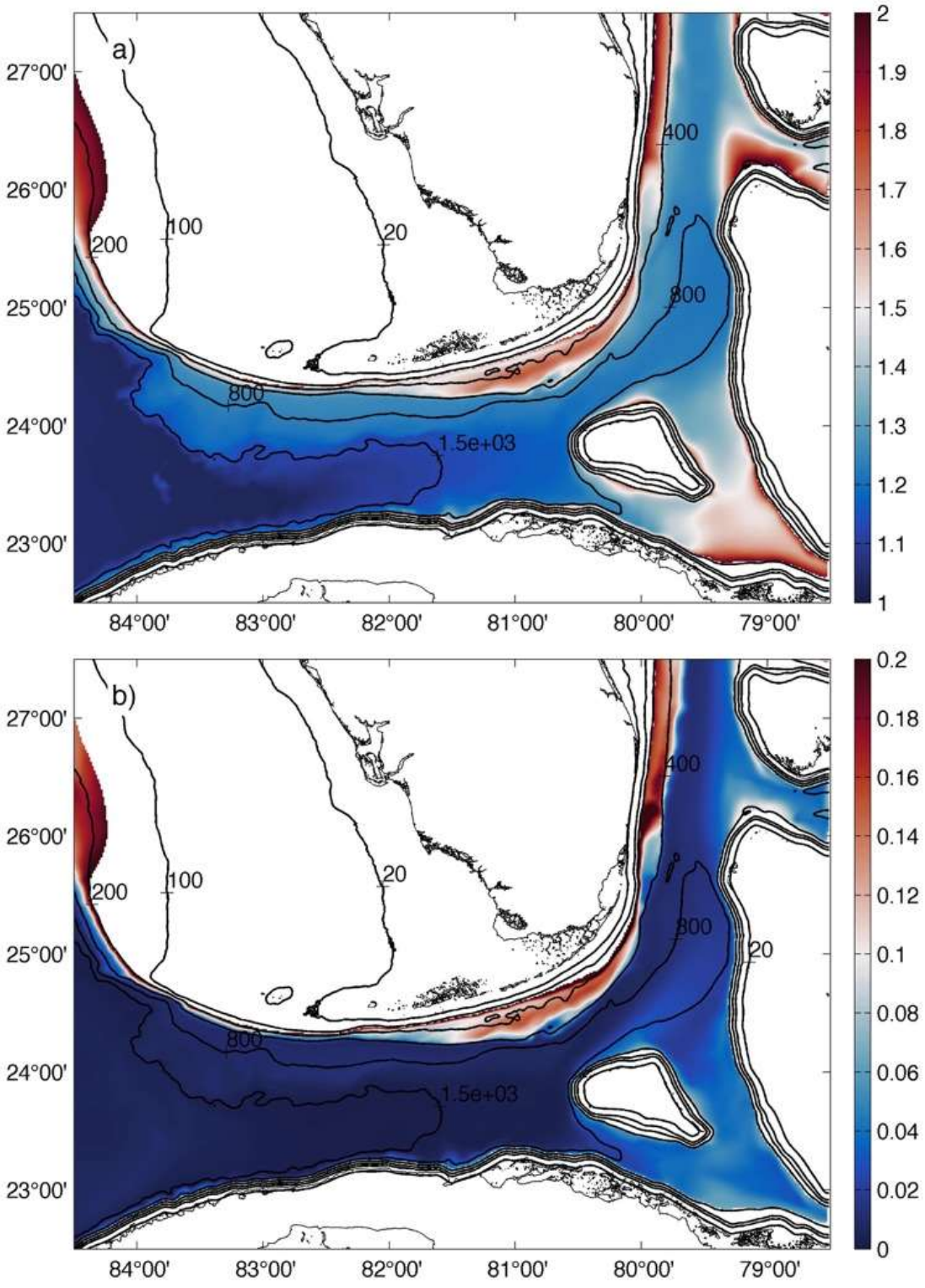

Figure 13. (top) Annual mean distribution of bottom Omega for 2012 and (bottom) the standard deviation of bottom Omega. Depth contours (black lines) are 20 m, 100 m, 200 m, 400 m, 800 m, and 1500 m.

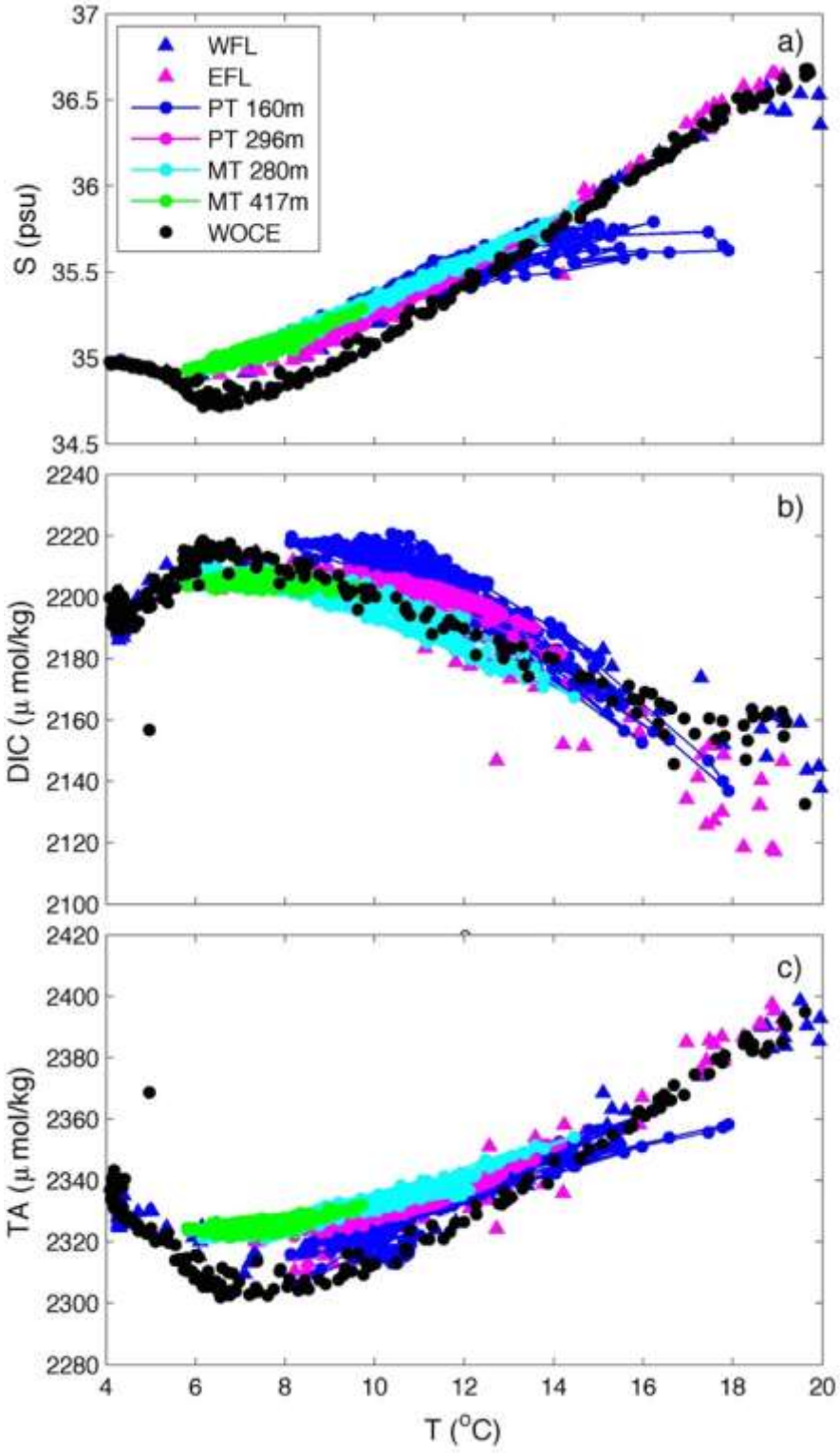

Figure 14. Temperature versus a) salinity, b) DIC, and c) TA along GOMECC2 WFL and EFL transects, at the four chosen sites on the Pourtalès and Miami Terraces (see Figure 1 for locations). Also shown are data from a subset of the WOCE A20 transect.

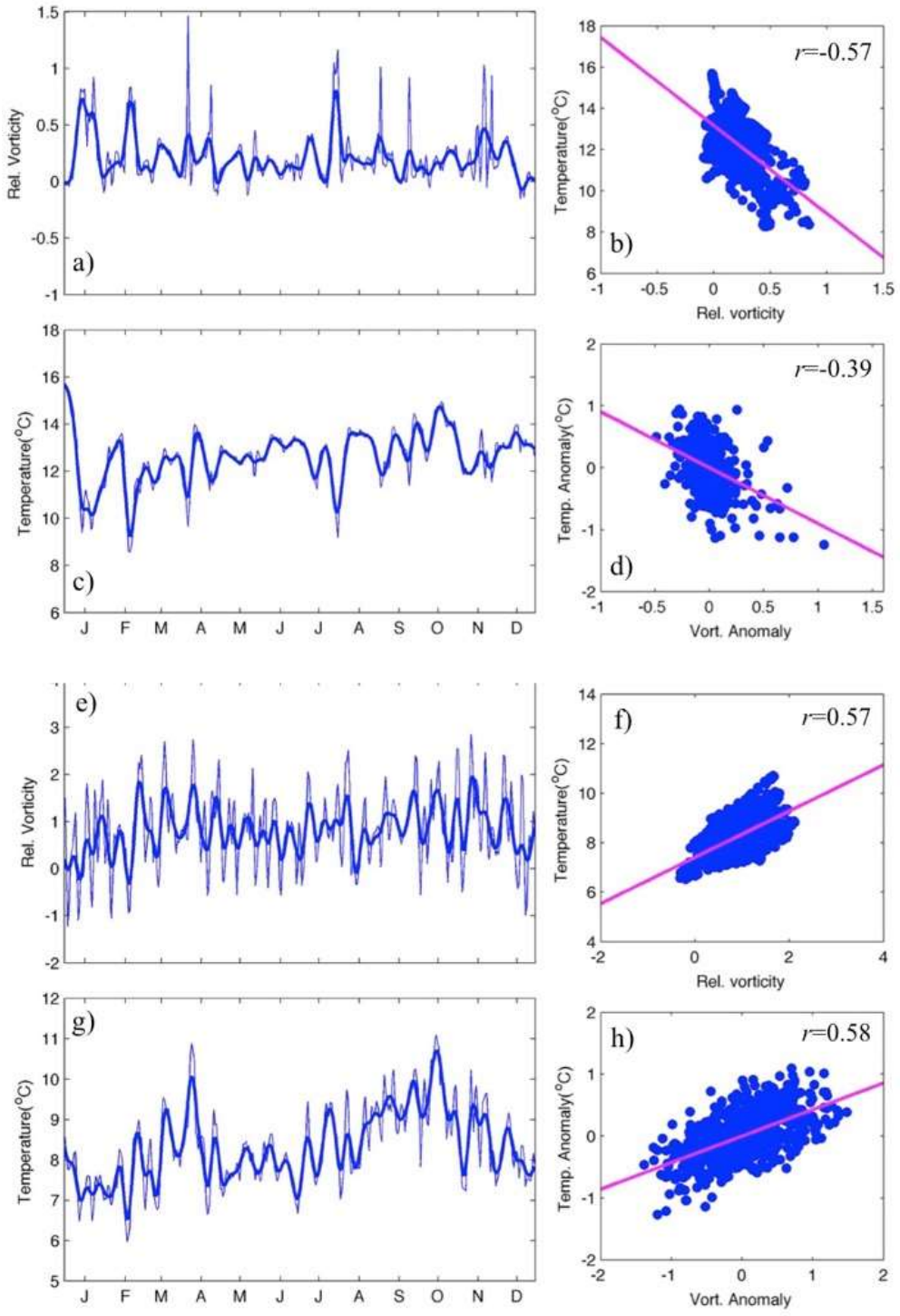

Figure 15. Modeled time-series of relative vorticity (ς) and near bottom temperature in 2012 for two sites on Pourtalès Terrace (296 m) and Miami Terrace (417 m): (a) ς at 150m and (c) bottom temperature on Pourtalès Terrace, (e) ς at 350 m and (g) bottom temperature on Miami Terrace. Their respective ς -T correlations for low-passed time-series (b and f) and anomalies (d, h) are shown on the right panels. Red lines on the right panels are the linear best fits for each pair.